LA-10192-MS

CIC-14 REPORT COLLECTION
REPRODUCTION
COPY

Los Alamos National Laboratory is operated by the University of California for the United States Department of Energy under contract W-7405-ENG-36

Plane-Wave Born Collision Strengths for Electron-Ion Excitation: Comparison with Other Theoretical Methods

LOS ALAMOS NATIONAL LABORATORY
3 9338 00318 6037

Los Alamos
Los Alamos National Laboratory
Los Alamos, New Mexico 87545

An Affirmative Action/Equal Opportunity Employer

This work was supported by the US Department of Energy, Office of Magnetic Fusion Energy.

DISCLAIMER

This report was prepared as an account of work sponsored by an agency of the United States Government. Neither the United States Government nor any agency thereof, nor any of their employees, makes any warranty, express or implied, or assumes any legal liability or responsibility for the accuracy, completeness, or usefulness of any information, apparatus, product, or process disclosed, or represents that its use would not infringe privately owned rights. Reference herein to any specific commercial product, process, or service by trade name, trademark, manufacturer, or otherwise, does not necessarily constitute or imply its endorsement, recommendation, or favoring by the United States Government or any agency thereof. The views and opinions of authors expressed herein do not necessarily state or reflect those of the United States Government or any agency thereof.

LA-10192-MS

UC-34a
Issued: September 1984

Plane-Wave Born Collision Strengths for Electron-Ion Excitation: Comparison with Other Theoretical Methods

R. E. H. Clark
L. A. Collins

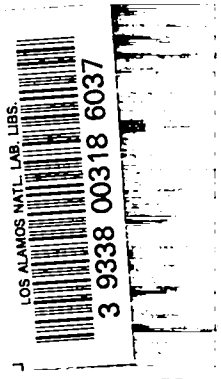

Los Alamos National Laboratory
Los Alamos, New Mexico 87545

PLANE-WAVE BORN COLLISION STRENGTHS FOR ELECTRON-ION EXCITATION: COMPARISON WITH OTHER THEORETICAL METHODS

by

R. E. H. Clark and L. A. Collins

ABSTRACT

Collision strengths and rates for electron-impact excitation of atomic ions are calculated in the plane-wave Born (PWB) approximation using the programs of Cowan and Robb. Two modifications of the PWB, which correct for the ionic threshold behavior, are investigated. Comparison is made with the distorted wave and Coulomb-Born-exchange techniques.

I. INTRODUCTION

The plane-wave Born (PWB) approximation[1] provides a simple, economical means of generating collision strengths for electronic excitations in atoms and ions due to electron impact. Since plane waves are employed and exchange effects are neglected, the method is strictly applicable only at high energies for spin-allowed transitions. However, in practice, the PWB collision strengths are in reasonable agreement (<30%) with those of other, more sophisticated methods such as the distorted wave (DW)[2] down to energies of a few times threshold. The prohibition against spin-forbidden transitions is valid only for pure-LS coupling. In general, the states consist of a mixture of LS terms, and thus the collision strength will not be zero due to the presence of a spin-allowed component. Since no explicit account is taken of the long-range Coulomb field, the threshold behavior for ionic targets is incorrect--going to

zero rather than a finite value. Through simple modifications of the near-threshold behavior of the PWB collision strength, this defect can be rectified. In many cases, these modified PWB collision strengths agree to better than a factor of 2 with the DW results even in the region near threshold.

In this report, we calculate PWB and modified PWB excitation collision strengths and rates for a variety of ionic targets using a program developed by Cowan and Robb. This program calculates the atomic wave functions and generalized oscillator strengths using the Hartree-Fock and configuration interaction codes of Cowan and determines the PWB collision strength from a subroutine of Robb. These results are compared with the distorted wave calculations of Mann[2] and the hydrogenic Coulomb-Born exchange (CBX) calculations of Sampson et al.[3] In Section II, we give a brief review of the PWB method while in Section III we describe the various calculations, listing the species, the transitions, and, where appropriate, the mixing coefficients of the CI calculation, the scaling parameters of the Coulomb integrals and spin-orbit component, and notes on any special features of the calculation. This section is followed by a brief discussion of the results (IV) and a series of the graphs, which gives the collision strengths for the various species and transitions under consideration as a function of the ratio (X) of the incident electron energy (k^2) to the threshold energy (ΔE). In addition, for selected transitions, we present the ratio of the PWB and CBX to the DW collision strengths as well as the rates as a function of temperature.

II. METHODS

The plane-wave Born (PWB) collision strength $\Omega_{\Gamma\Gamma'}(X)$ for a transition between initial and final levels Γ and Γ' respectively is given by [1]

$$\Omega^{PWB}_{\Gamma\Gamma'}(X) = \frac{8}{k^2} \int_{k_{min}}^{k_{max}} gf_{\Gamma\Gamma'}(K)\, d(\ln K) \quad , \tag{1}$$

where k^2 is the energy of the incident electron in Rydbergs, $(k')^2$ is the energy of the outgoing electron $[(k')^2 = k^2 - \Delta E]$, ΔE is the threshold energy, $gf_{\Gamma\Gamma'}$ is the generalized oscillator strength (see Ref. 1, Secs. 18-12), and X is the ratio of the incident and threshold energies ($X = k^2/\Delta E$). The momentum transfer K over which the integration is performed is defined by

$$\vec{K} = \vec{k}' - \vec{k} \quad ,$$

with the limits given by

$$K_{\substack{min \\ max}} = k \mp k' \quad .$$

The label of the level consists of the total angular momentum quantum number J plus a designation α describing all other quantum numbers and the configuration that specify the level. For ions, the PWB form has been modified in order to give a more realistic threshold behavior. The two modified forms employed in this study are given by[1]

$$\Omega^{M1}(X) = \Omega^{PWB}(3)\, F(X) \quad , \text{ and} \tag{2}$$

$$\Omega^{M2}(X) = \Omega^{PWB}(X + 3/(1 + X)) \quad , \tag{3}$$

where

$$F(X) \equiv 1. - 0.2 \exp(0.07702\,(1 - X)) \quad .$$

Most of the collision strengths considered in Section III involve transitions between single values of J in the initial and final levels. For cases involving several J values, we present the summed collision strength $\Omega_{\alpha\alpha'}$ given by

$$\Omega_{\alpha\alpha'}(X) = \sum_{JJ'} \Omega_{\alpha J, \alpha' J'} \quad . \tag{4}$$

The PWB collision strengths were obtained from the structure programs of Cowan (RCN31, RCN2, RCG8), which have been modified by Robb to produce the scattering information. For some of the transitions under consideration, we also calculate the rate coefficients as a function of electron temperature T. The rates are determined by integrating the cross section over a Boltzmann distribution.

III. DESCRIPTION OF CALCULATIONS

In this section, we give a description of the systems for which calculations were performed. For all cases, we give the transitions and configurations employed. For certain transitions, we also include the CI mixing coefficients generated by RCG8 as well as the scaling parameters of the Coulomb integrals. ($F^k(\ell_i,\ell_i)$, $F^k(\ell_i,\ell_j)$, $G^k(\ell_i,\ell_j)$, and $R^k(\ell_i\ell_j,\ell_{i'}\ell_{j'})$) and the spin-orbit term (ζ_i).[1] Where appropriate, additional comments are supplied to clarify the precise nature of the calculation. The figure numbers associated with each transition are also given.

A. Lithium-like

C IV

Transitions: 2s → 2p — Fig. 1

Configurations: [He] 2s ; 2p

Note: An atomic symbol in brackets is used to denote the closed-shell core of the ion under consideration. For example [He] 2s implies a full configuration of $1s^2 2s$.

Si XII

Transitions: 2s → 2p — Fig. 2

Configurations: [He] 2s ; 2p

Ar XVI

Transitions: 2s → 2p — Fig. 3

Configurations: [He] 2s ; 2p

Fe XXIV

Transitions:

a)	2s → 2p	Fig. 4a,b
b)	2s → 3s	Fig. 5a,b,c
c)	2s → 3p	Fig. 6a,b,c
d)	2s → 3d	Fig. 7a,b,c

Configurations: a) [He] 2s ; 2p
b) [He] 2s ; 3s
c) [He] 2s ; 3p
d) [He] 2s ; 3d

Notes: For purposes of comparison, the collision strengths for the 2s → 2p transition are summed at the same value of X even though the $P_{1/2}$ and $P_{3/2}$ levels have different thresholds, $\Delta E(^2S_{1/2} - {}^2P_{1/2}) = 3.574$ Ry; $\Delta E(^2S_{1/2} - {}^3P_{3/2}) = 4.752$ Ry.

Mo XL

Transitions: 2s → 2p Fig. 8

Configurations: [He] 2s , 2p

Notes: For purposes of comparison, the collision strengths for the $^2P_{1/2}$ and $^2P_{3/2}$ transitions are summed at the same value of X [$\Delta E(^2S_{1/2} - {}^2P_{1/2}) = 6.184$ Ry; $\Delta E(^2S_{1/2} - {}^2P_{3/2}) = 15.605$ Ry].

B. Beryllium-like

C III

Transitions: a) $2s^2 \rightarrow 2s2p\ {}^1P$ Fig. 9
b) $2s^2 \rightarrow 2s2p\ {}^3P$ Fig. 10

Configurations: a-b) [He] $2s^2$; 2s2p ; $2p^2$

Mixing Coefficients:

a) initial state J=0 ^1S
$2s^2\ {}^1S$ -0.96819
$2p^2\ {}^3P$ -0.00014

b) final state J=1 ^1P
$2s2p\ {}^1P$ 0.99999
$2s2p\ {}^3P$ 0.00075

Scaling Coefficients: 0.85, 0.85, 0.85, 0.85, 1.00

Fe XXIII

Transitions:

a)	$2s^2 \rightarrow 2s2p\ ^1P$	Fig. 11a,b
b)	$2s^2 \rightarrow 2s2p\ ^3P$	Fig. 12a,b
c)	$2s^2 \rightarrow 2s3s\ ^1S$	Fig. 13a,b,c
d)	$2s^2 \rightarrow 2s3p\ ^1P$	Fig. 14a,b,c
e)	$2s^2 \rightarrow 2s3p\ ^3P$	Fig. 15a,b
f)	$2s^2 \rightarrow 2s3d\ ^1D$	Fig. 16a,b,c

Configurations:

a-b) [He] $2s^2$; 2s2p ; $2p^2$

c) [He] $2s^2$; 2s3s ; 2p3p ; $2p^2$

d-e) [He] $2s^2$; 2s3p ; 2p3s ; 2p3d ; $2p^2$

f) [He] $2s^2$; 2s3d ; 2p3p ; $2p^2$

Mixing Coefficients:

a) initial state J=0 ^1S

$2s^2\ ^1S$	0.97940
$2p^2\ ^3P$	0.02390
$2p^2\ ^1S$	0.20052

b) final state J=1 ^3P

$2s2p\ ^3P$	0.98691
$2s2p\ ^1P$	0.16126

Scaling Coefficients:

a-b) 0.95, 0.95, 0.95, 0.95, 1.00

c-d) 0.87, 0.87, 0.87, 0.87, 1.00

Notes: Since the PWB formulation does not contain exchange effects, the collision strength for spin-forbidden transitions between unmixed states is zero. This is not the case for the $^1S \rightarrow ^3P$ transition in Fe XXIII due to the mixing of the ^3P and ^1P levels.

C. Neon-like

Al IV

Transitions:

a)	$2p^6 \rightarrow 2p^5 3s\ ^1P$	Fig. 17
b)	$2p^6 \rightarrow 2p^5 3s\ ^3P$	Fig. 18

Configurations: a-b) [He] $2s^2 2p^6$; $2s^2 2p^5 3s$

Mixing Coefficients:

final state	J=1 ^1P
$2p^5 3s\ ^3P$	0.31083
$2p^5 3s\ ^1P$	-0.95047

Scaling Coefficients: 0.80, 0.80, 0.80, 0.80, 1.00

Fe XVII

Transitions: a) $2p^6 \rightarrow 2p^5 3s\ ^1P$ Fig. 19 a,b

b) $2p^6 \rightarrow 2p^5 3s\ ^3P$ Fig. 20 a,b

Configurations: a-b) [He] $2s^2 2p^6$; $2s^2 2p^5 3s$; $2s^2 2p^5 3d$; $2s^1 2p^6 3p$

Mixing Coefficients:

final state	J=1 ^1P
$2p^5 3s\ ^3P$	0.66556
$2p^5 3s\ ^1P$	0.74545
$2p^5 3d\ ^3P$	-0.00745
$2p^5 3d\ ^1P$	-0.02442
$2p^5 3d\ ^3D$	0.00174
$2s2p^6 3p\ ^3P$	-0.02125
$2s2p^6 3p\ ^1P$	-0.01496

Scaling Coefficients: a) 0.90, 0.90, 0.90, 0.80, 1.00

Notes: The spin-forbidden PWB collision strength is nonzero due to the triplet-singlet mixing in the final state wave function.

D. Sodium-like

Fe XVI

Transitions: a) 3s → 3p Fig. 21

b) 3s → 4s Fig. 22

Configurations: a) [Ne] 3s ; 3p

b) [Ne] 3s ; 4s

E. Aluminum-like

Ti X

Transitions: a) $3s^2 3p \rightarrow 3s3p^2\ ^2D$ Fig. 23

b) $3s^2 3p \rightarrow 3s^2 3d^1\ ^2D$ Fig. 24

Configurations: a-b) [Ne] $3s^2 3p$; $3s3p^2$, $3s^2 3d$

Mixing Coefficients:

final state	J=-3/2
$3s^2 3d^1\ ^2D$	0.95040
$3s^1 3p^2\ ^2D$	0.30797
$3s^1 3p^2\ ^2P$	0.03773
$3s^1 3p^2\ ^4P$	0.02181

Scaling Coefficients: 0.90, 0.90, 0.90, 0.90, 1.00

IV. DISCUSSION

The figures, which compare the various calculational methods, are reasonably self-explanatory and present a broad comparison for different types of systems and transitions. Therefore, we are relieved of presenting a detailed discussion of the results and instead concentrate on the major conclusions that can be drawn from this comparison. These conclusions are as follows: (1) The M2 modified PWB prescription generally gives the best agreement with the DW results. The exceptions to this rule involve s- to d-type transitions [Fe XXIV $2s \rightarrow 3d$ and Fe XXIII $2s^2 \rightarrow 2s3d\ ^1D$] although these differences disappear by energies of 10 times threshold (X = 10). (2) The M2-PWB agrees with the DW to within better than thirty percent (30%) for energies above a few times threshold (X = 2 - 3). The exceptions to this condition are the spin-forbidden transitions for weakly coupled systems [C III $2s^2 - 2s2p\ ^3P$ and Fe XXIII $2s^2 - 2s2p\ ^3P$]. (3) For energies near threshold ($X \lesssim 1 - 2$), the M2-PWB results are usually within better than a factor of 2 of the DW. The most pronounced exception to this rule comes from the spin-forbidden transition in A IV ($2p^6 \rightarrow 2p^5 3s\ ^3P$) in which the exchange contribution dominates that of the mixing at low energies. (4) Spin-forbidden transitions are given reasonably well by the M2-PWB provided that the states are sufficiently mixed. We can see this by viewing the progression from C III to Fe XXIII to Fe XVII. For C III the triplet-singlet mixing is negligible, and the spin-forbidden transition is

practically zero. The amount of singlet component in the Fe XXIII ^3P wave function is about 3% while for Fe XVII this value has risen to nearly 45%. As expected, the agreement improves as the mixing becomes stronger. (5) The M2-PWB rates in general agree with those of the DW to better than 30% over a range of temperatures from 0 to 10^4 K. The exception again occurs for transitions involving a d-type configuration with the largest difference being on the order of 50%.

REFERENCES

[1] R. D. Cowan, The Theory of Atomic Structure and Spectra (University of California Press, Berkeley, 1981).

[2] J. B. Mann, At. Data Nucl. Data Tables 29, 409 (1983); A. L. Merts, J. B. Mann, W. D. Robb, and N. H. Magee, "Electron Excitation Collision Strengths for Positive Atomic Ions: A Collection of Theoretical Data," Los Alamos Scientific Laboratory report LA-8267-MS (1980).

[3] D. H. Sampson, S. J. Goett, R. E. H. Clark, At. Data Nucl. Data Tables 30, 125 (1984); L. B. Golden, R. E. H. Clark, S. J. Goett, and D. H. Sampson, Astrophys. J. Suppl. 45, 603 (1981).

FIGURES

The basic figure is a plot of the collision strength $\Omega_{ii'}$ as a function of X, the ratio of the incident energy of the electron to the threshold energy. The species and transition are given at the top of the graph. The PWB, modified PWB (M1, M2), DW, and CBX collision strengths are plotted in a consistent notation throughout the set. For some transitions, we present a second graph which gives the ratio of the PWB and CBX collision strengths to that of the DW as a function of X. In addition, the rate coefficients are present for a selected set of transitions. The notation is as follows:

\- - - Plane-Wave Born (PWB)

o o PWB (M1)

+ + PWB (M2)

Δ Δ Coulomb-Born Exchange (CBX)

—— Distorted Wave (DW)

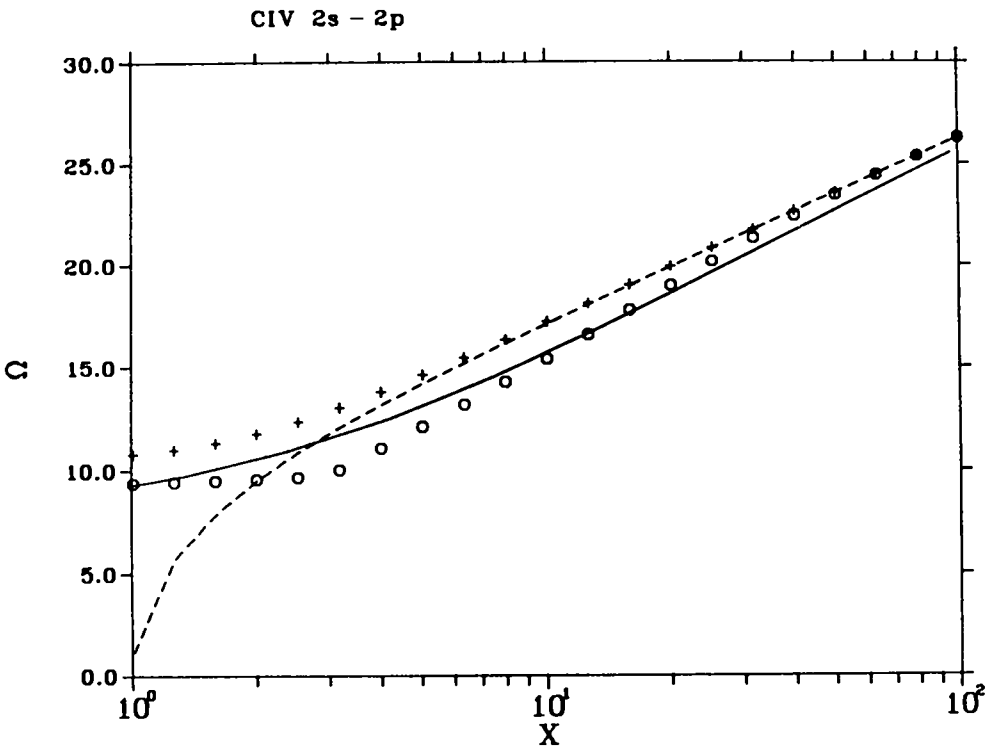
CIV 2s - 2p
30.0
25.0
20.0
15.0
10.0
5.0
0.0
C
10^0
10^1
10^2
X

Fig. 1.

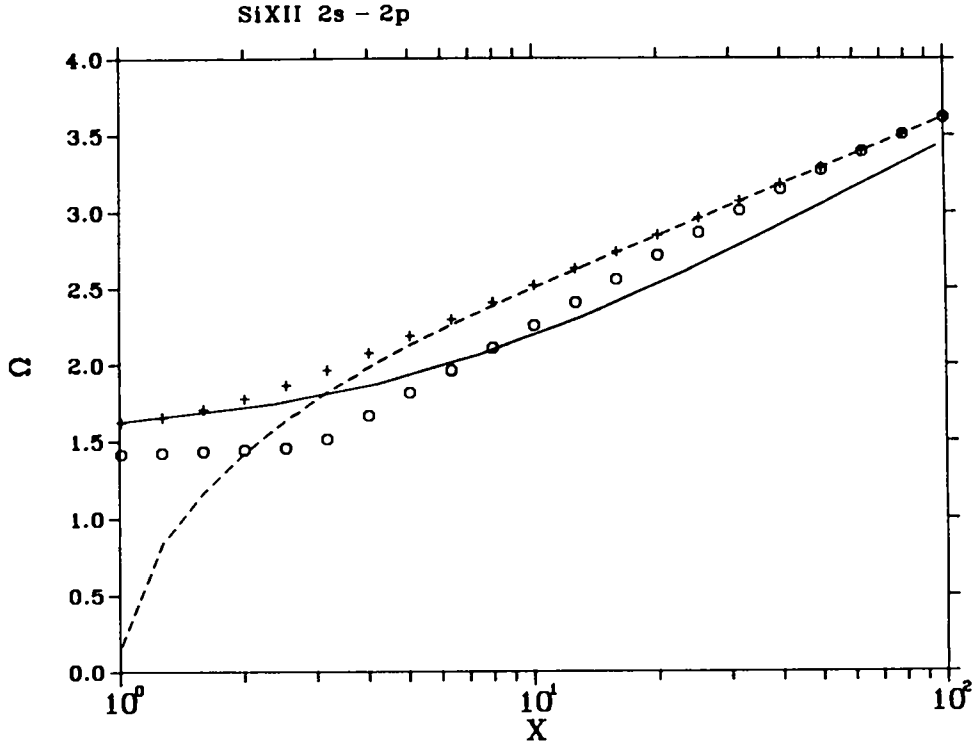
SiXII 2s - 2p
4.0
3.5
3.0
2.5
2.0
1.5
1.0
0.5
0.0
C
10^0
10^1
10^2
X

Fig. 2.

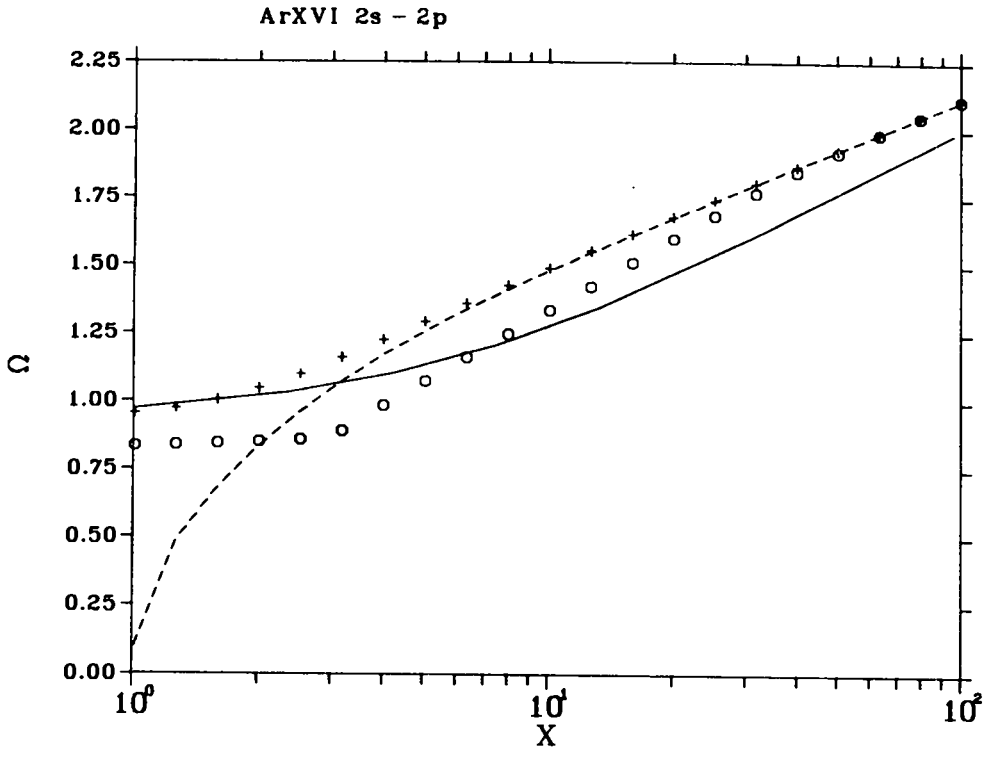
ArXVI 2s - 2p
2.25
2.00
1.75
1.50
1.25
1.00
0.75
0.50
0.25
0.00
Ω
10^0
10^1
10^2
X

Fig. 3.

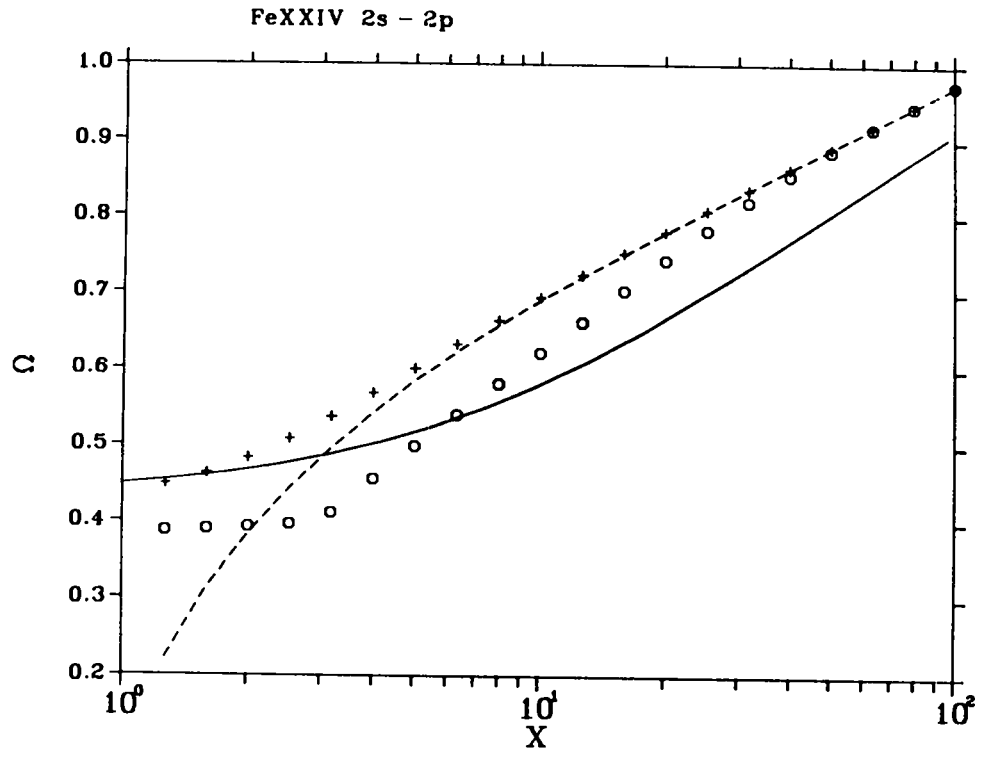
FeXXIV 2s - 2p
1.0
0.9
0.8
0.7
0.6
0.5
0.4
0.3
0.2
Ω
10^0
10^1
10^2
X

Fig. 4a.

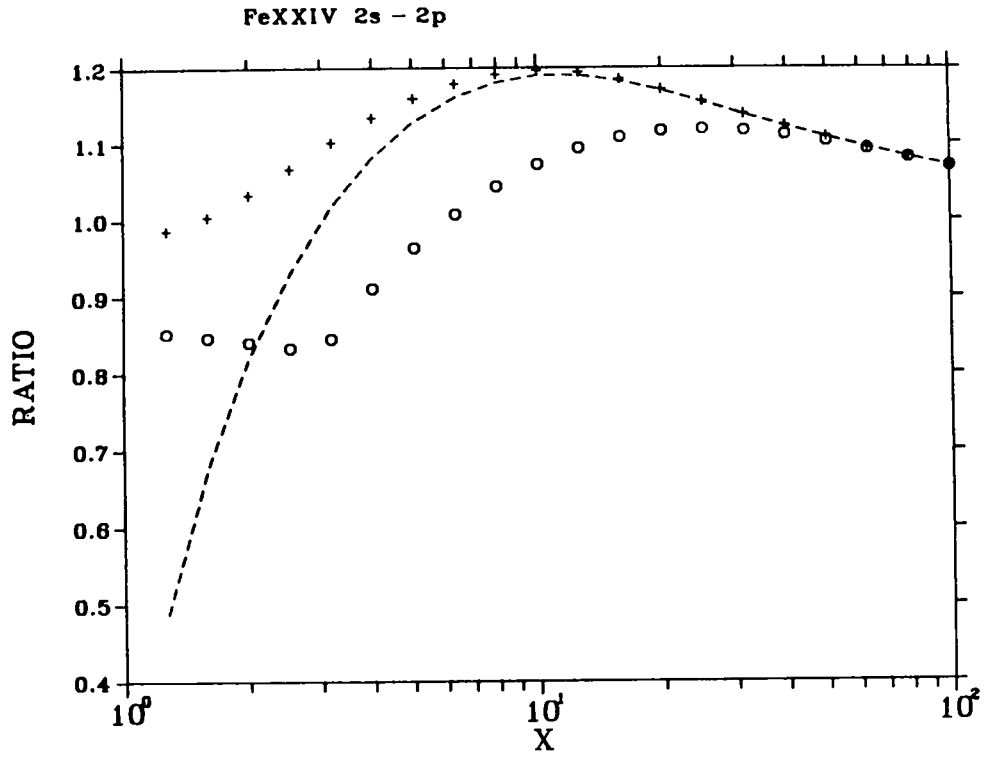
FeXXIV 2s - 2p
RATIO
X
1.2
1.1
1.0
0.9
0.8
0.7
0.6
0.5
0.4
10⁰
10¹
10²

Fig. 4b.

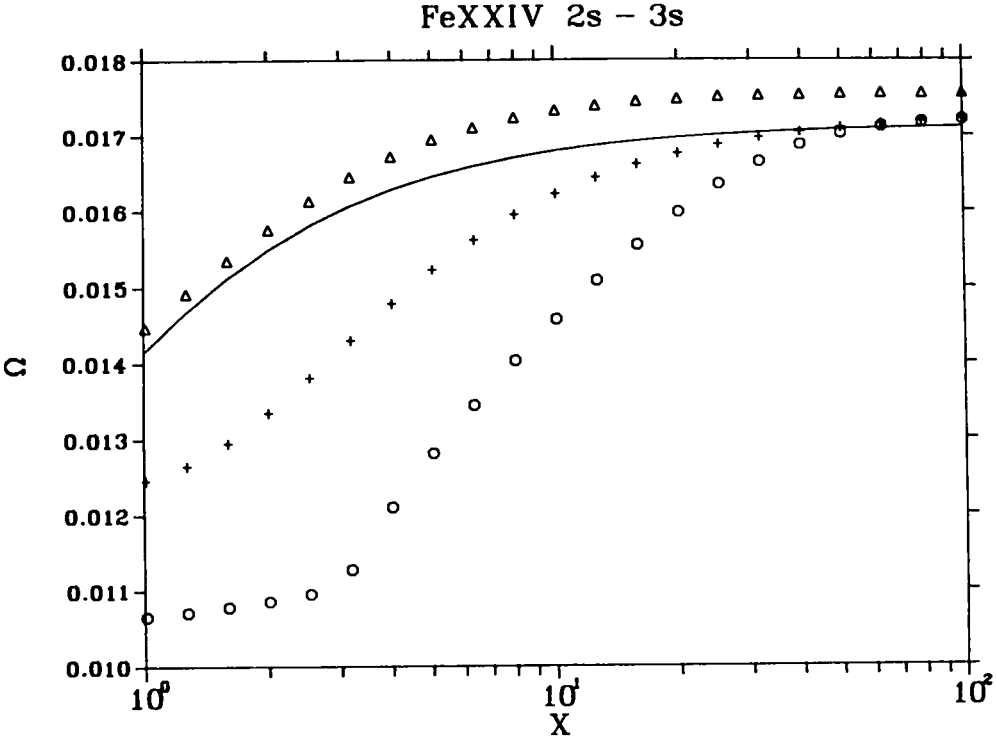
FeXXIV 2s - 3s
Ω
X
0.018
0.017
0.016
0.015
0.014
0.013
0.012
0.011
0.010
10⁰
10¹
10²

Fig. 5a.

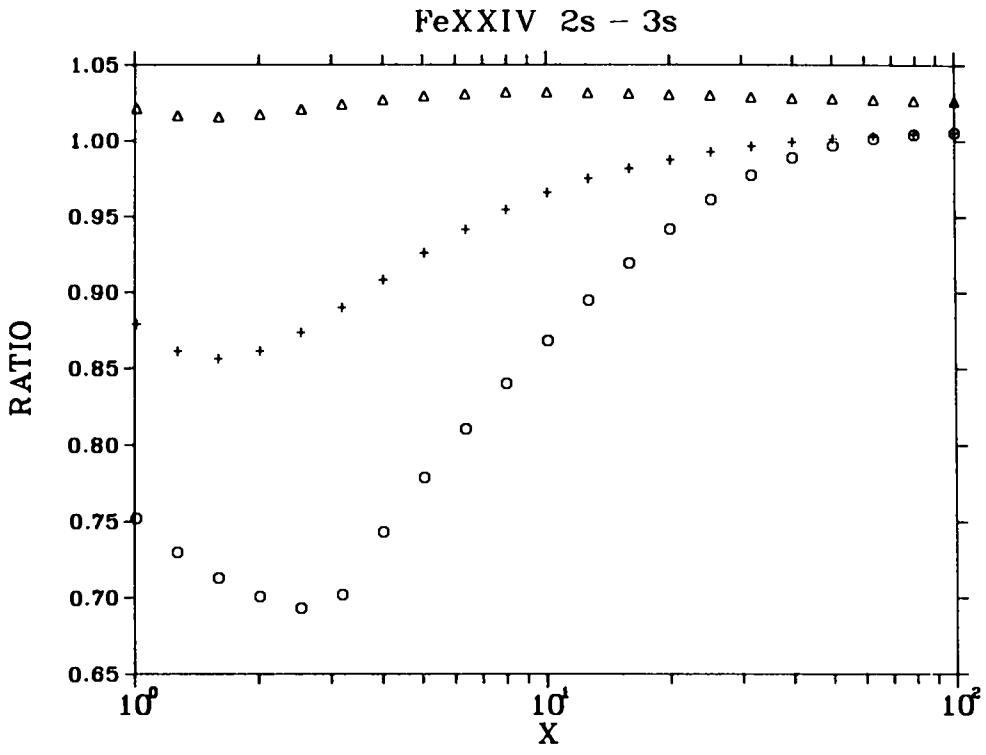
FeXXIV 2s – 3s
RATIO
1.05
1.00
0.95
0.90
0.85
0.80
0.75
0.70
0.65
10^0
10^1
10^2
X

Fig. 5b.

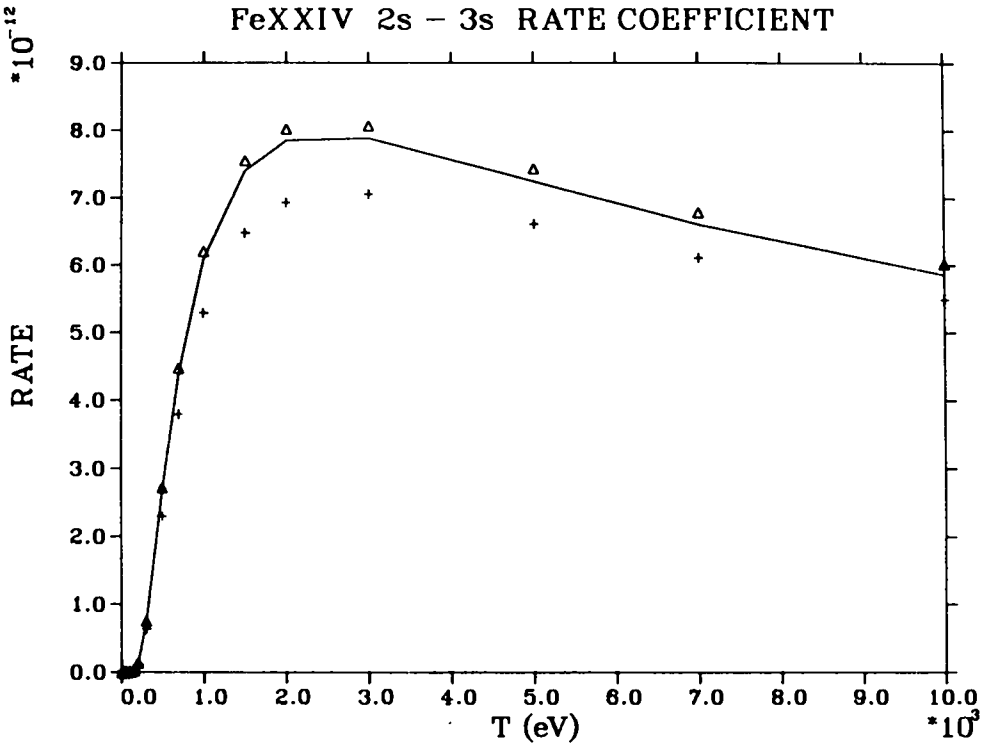
FeXXIV 2s – 3s RATE COEFFICIENT
*10^-12
RATE
9.0
8.0
7.0
6.0
5.0
4.0
3.0
2.0
1.0
0.0
0.0
1.0
2.0
3.0
4.0
5.0
6.0
7.0
8.0
9.0
10.0
T (eV)
*10^3

Fig. 5c.

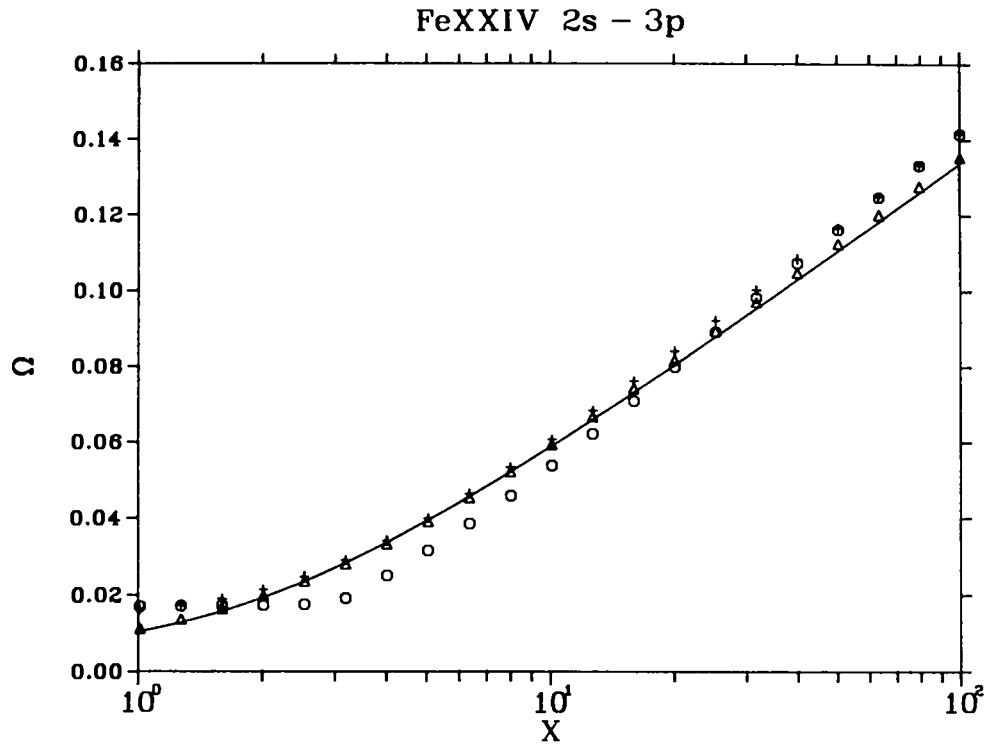
FeXXIV 2s – 3p
Ω
X
0.16
0.14
0.12
0.10
0.08
0.06
0.04
0.02
0.00
10⁰
10¹
10²

Fig. 6a.

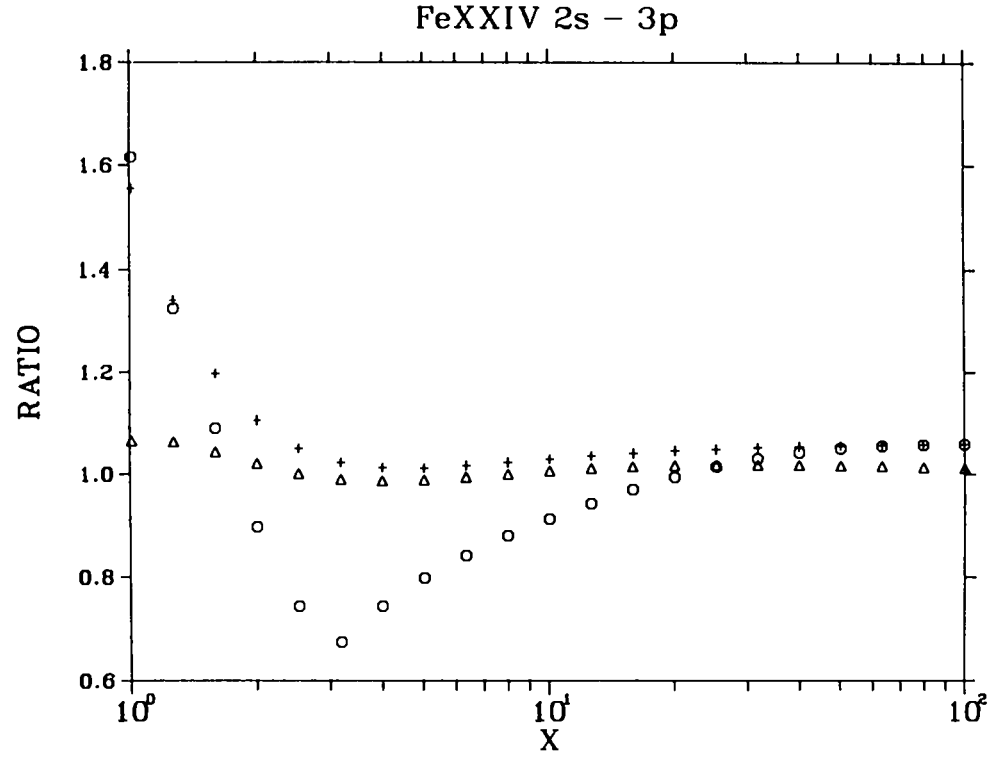
FeXXIV 2s – 3p
RATIO
X
1.8
1.6
1.4
1.2
1.0
0.8
0.6
10⁰
10¹
10²

Fig. 6b.

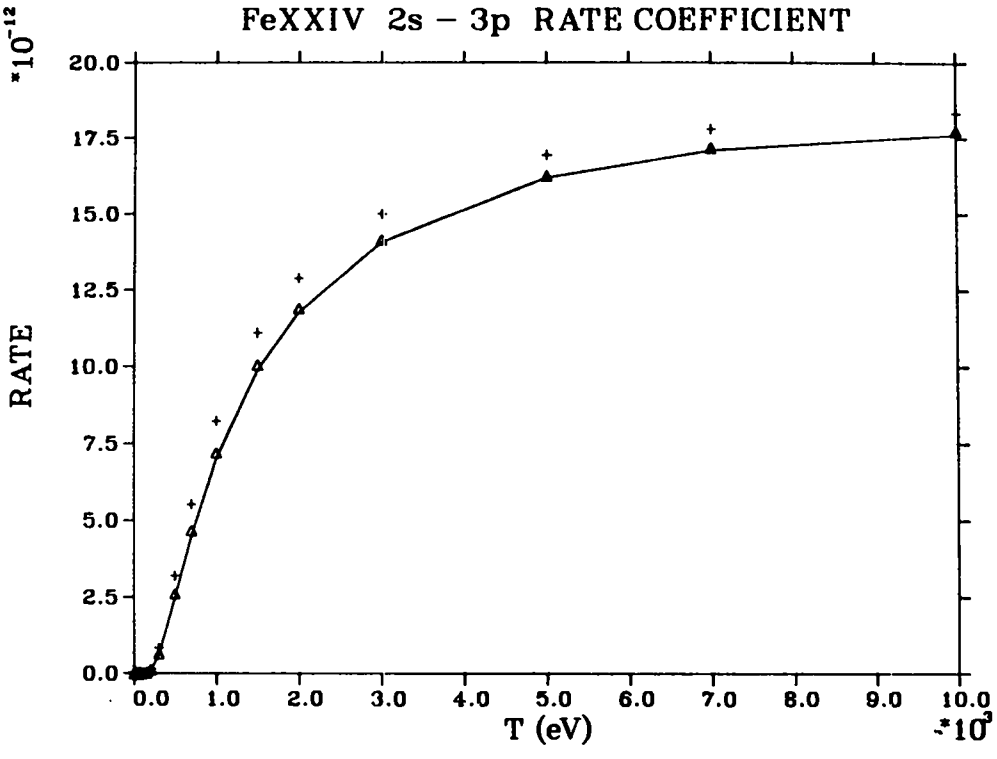
FeXXIV 2s – 3p RATE COEFFICIENT
*10⁻¹²
RATE
20.0
17.5
15.0
12.5
10.0
7.5
5.0
2.5
0.0
0.0
1.0
2.0
3.0
4.0
5.0
6.0
7.0
8.0
9.0
10.0
T (eV)
*10³

Fig. 6c.

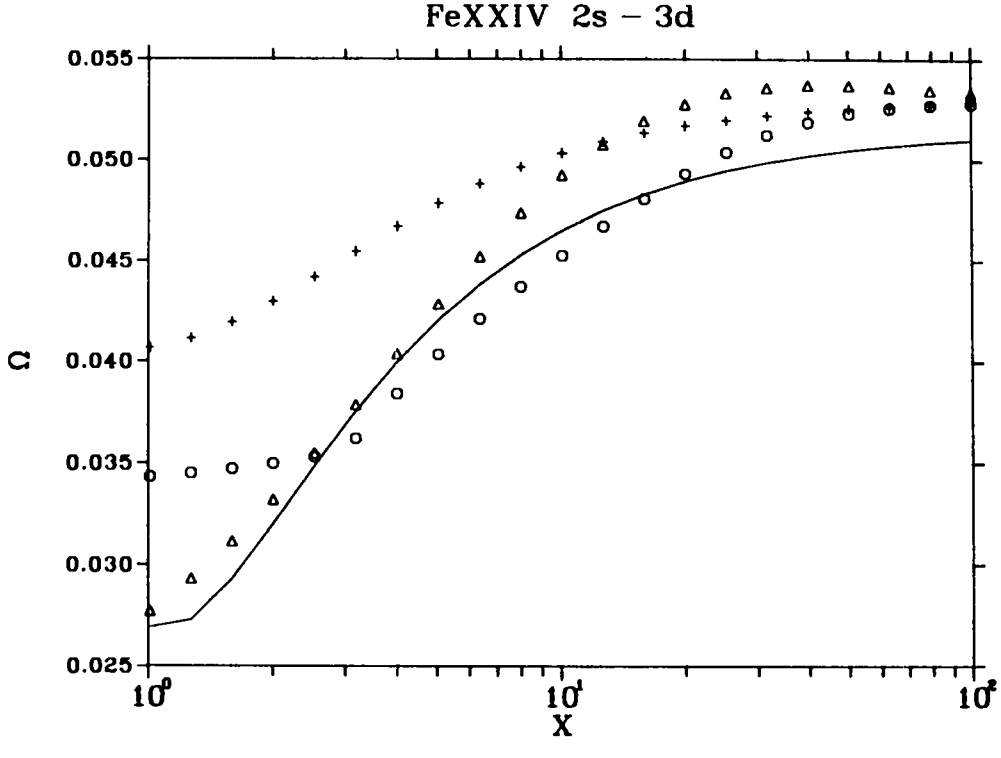
FeXXIV 2s – 3d
Ω
0.055
0.050
0.045
0.040
0.035
0.030
0.025
10⁰
10¹
10²
X

Fig. 7a.

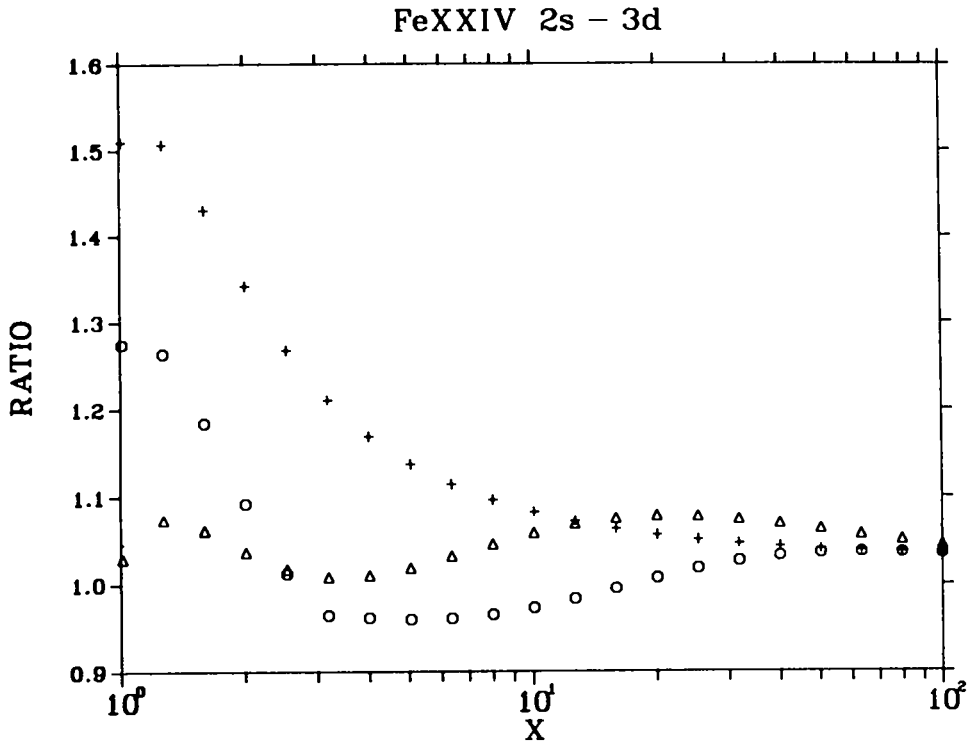
FeXXIV 2s – 3d
RATIO
X
1.6
1.5
1.4
1.3
1.2
1.1
1.0
0.9
10^0
10^1
10^2

Fig. 7b.

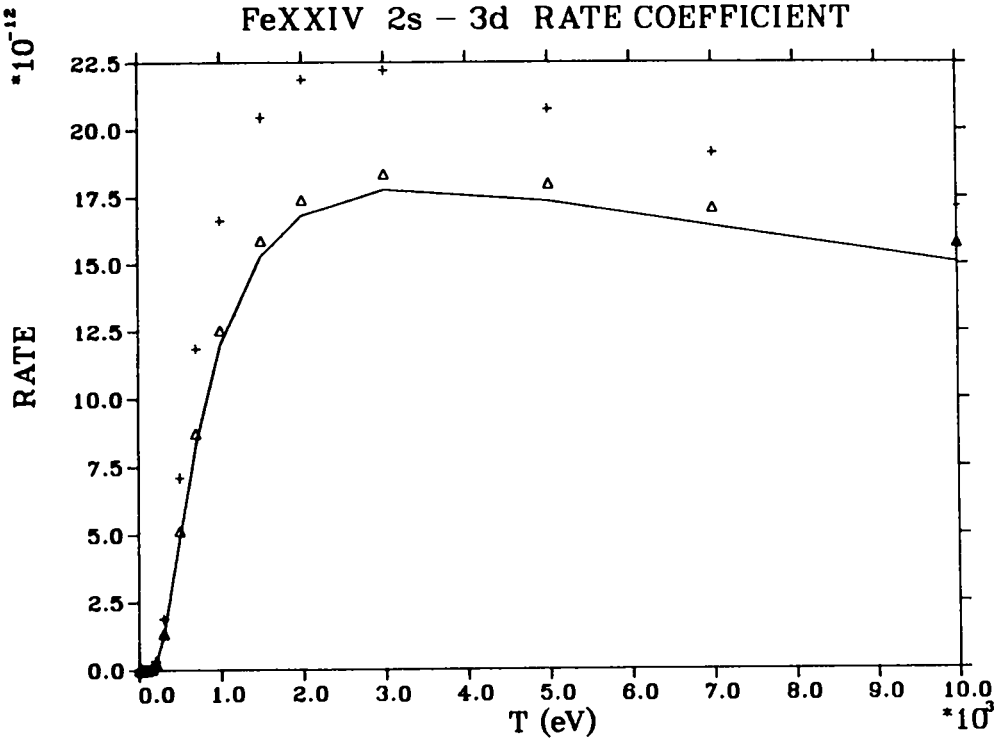
FeXXIV 2s – 3d RATE COEFFICIENT
*10^-12
RATE
T (eV)
*10^3
22.5
20.0
17.5
15.0
12.5
10.0
7.5
5.0
2.5
0.0
0.0
1.0
2.0
3.0
4.0
5.0
6.0
7.0
8.0
9.0
10.0

Fig. 7c.

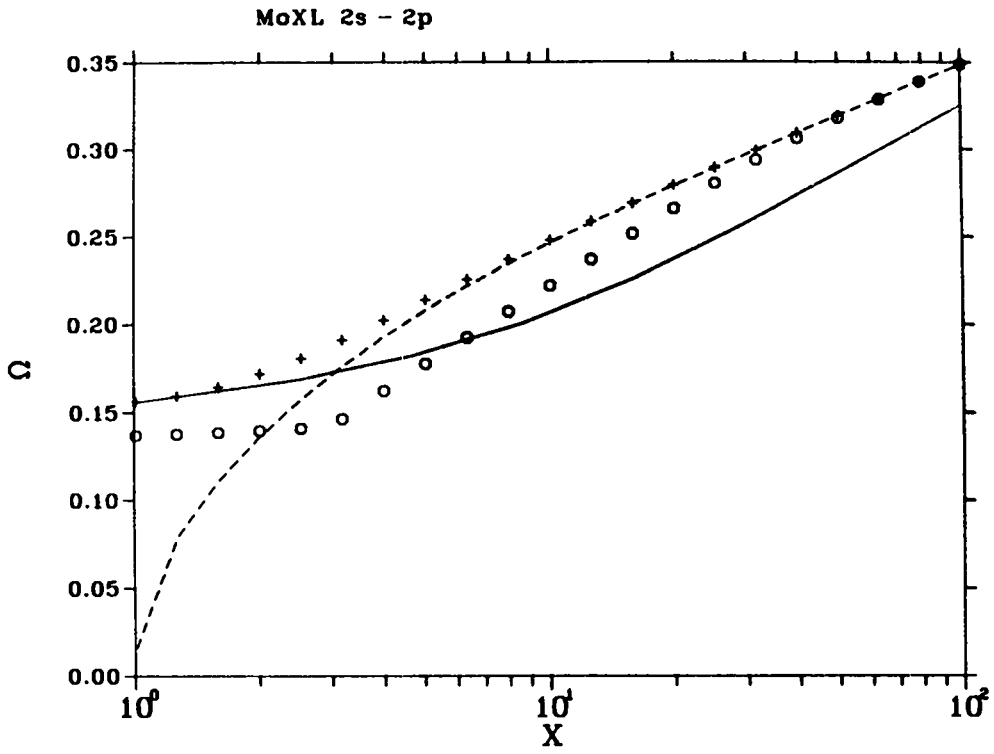
MoXL 2s - 2p
0.35
0.30
0.25
0.20
0.15
0.10
0.05
0.00
C
10^0
10^1
10^2
X

Fig. 8.

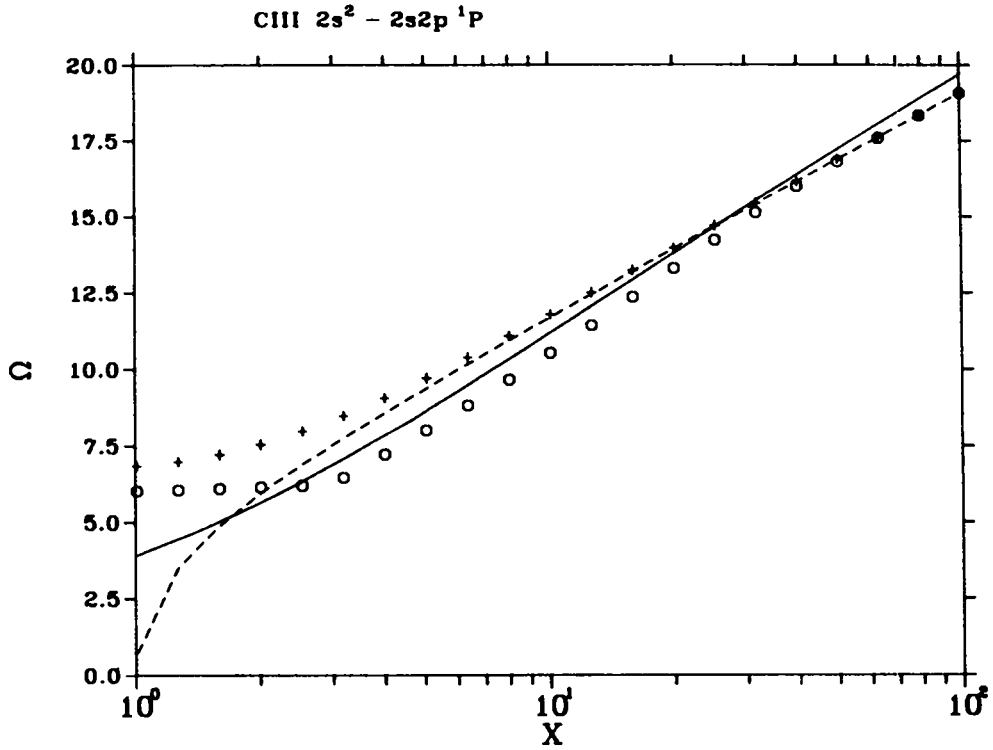
CIII $2s^2$ - 2s2p ^1P
20.0
17.5
15.0
12.5
10.0
7.5
5.0
2.5
0.0
C
10^0
10^1
10^2
X

Fig. 9.

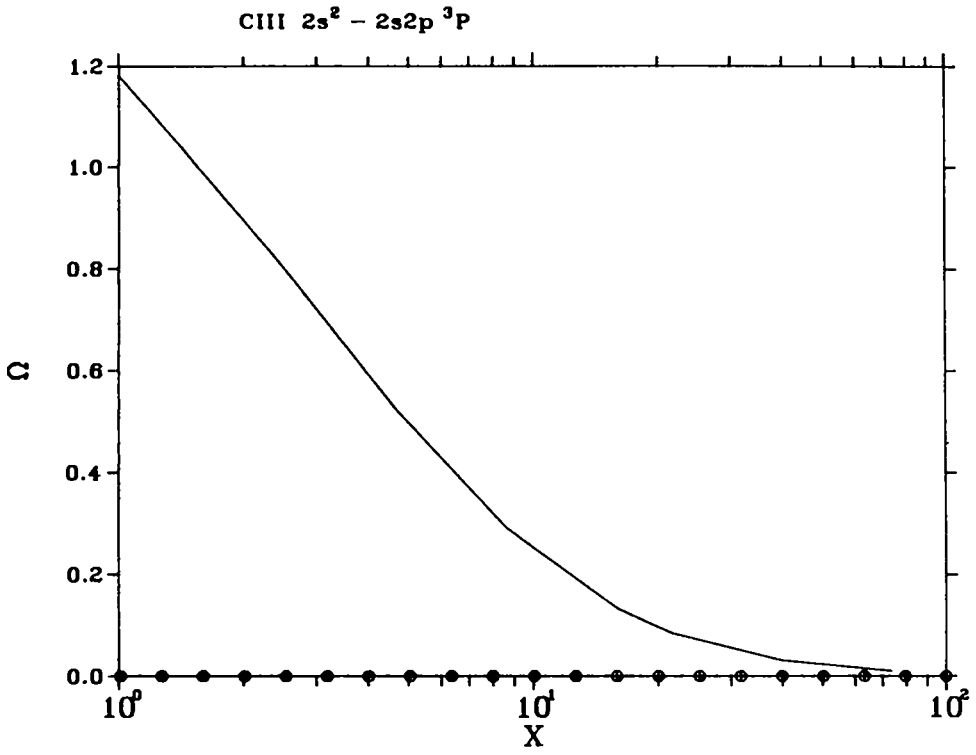

Fig. 10.

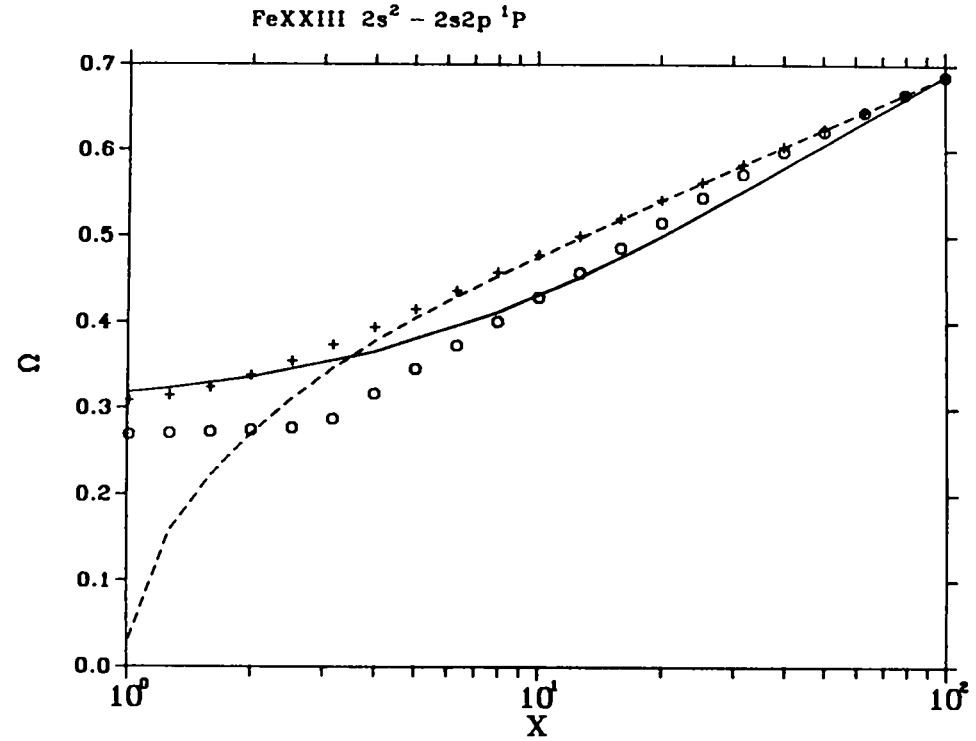

Fig. 11a.

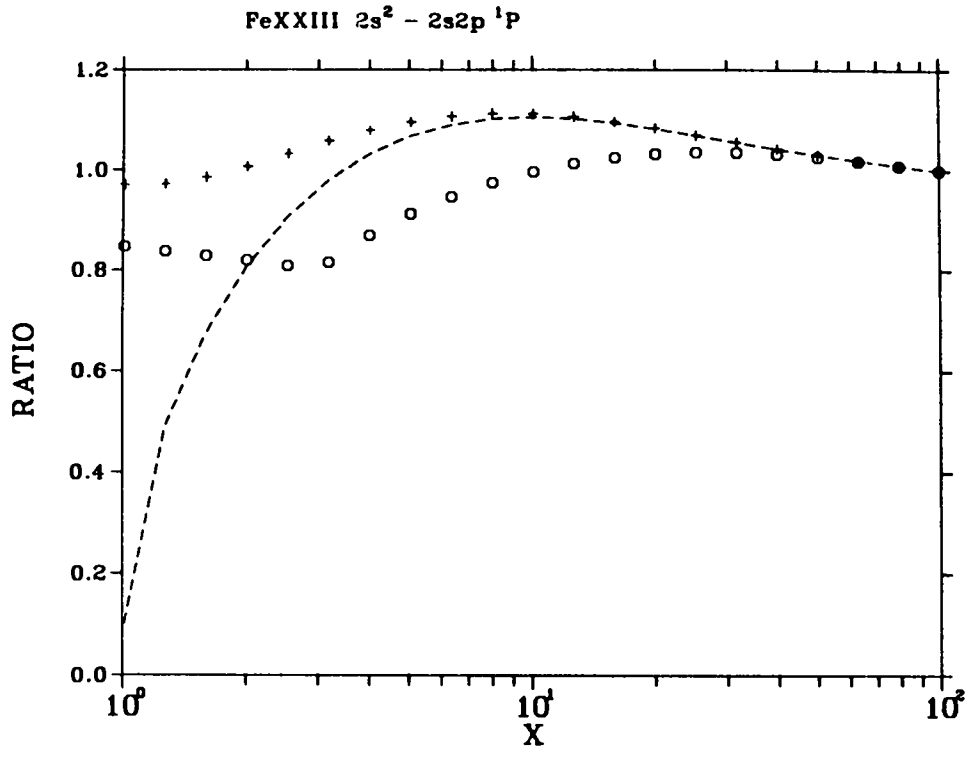

Fig. 11b.

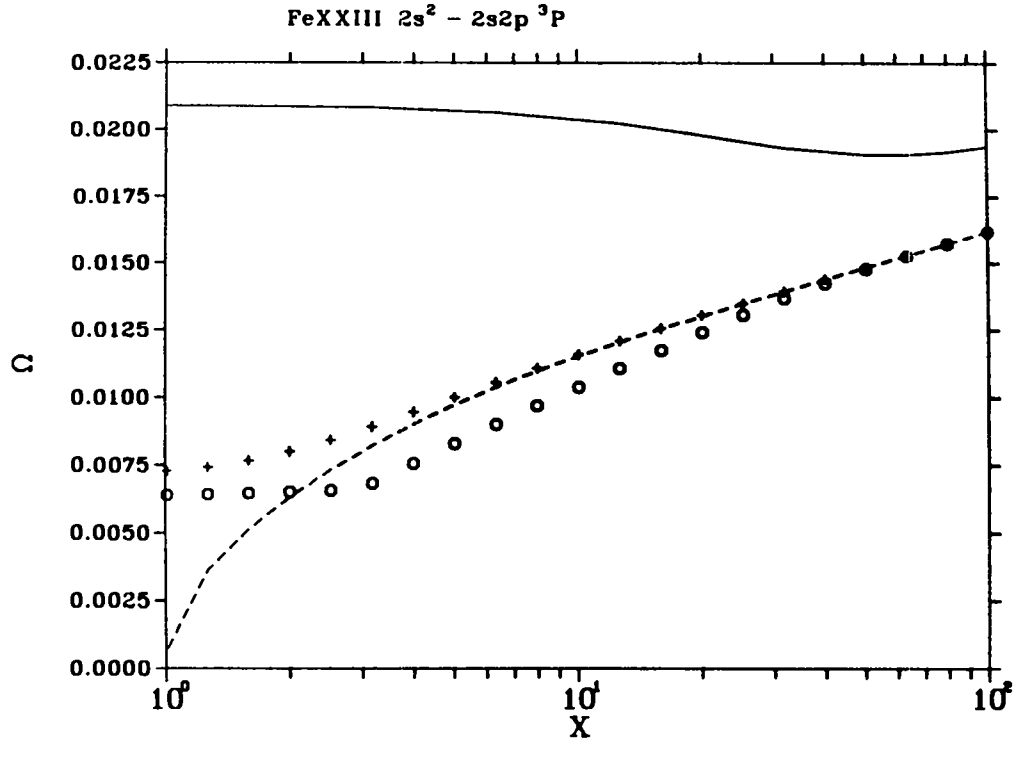

Fig. 12a.

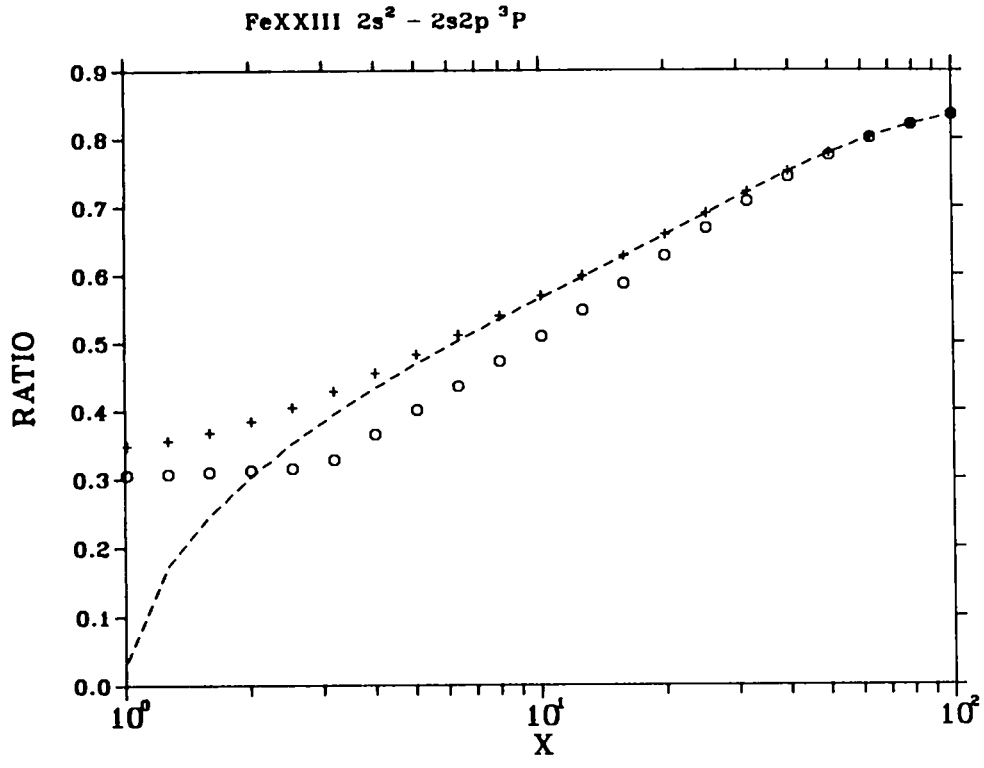

Fig. 12b.

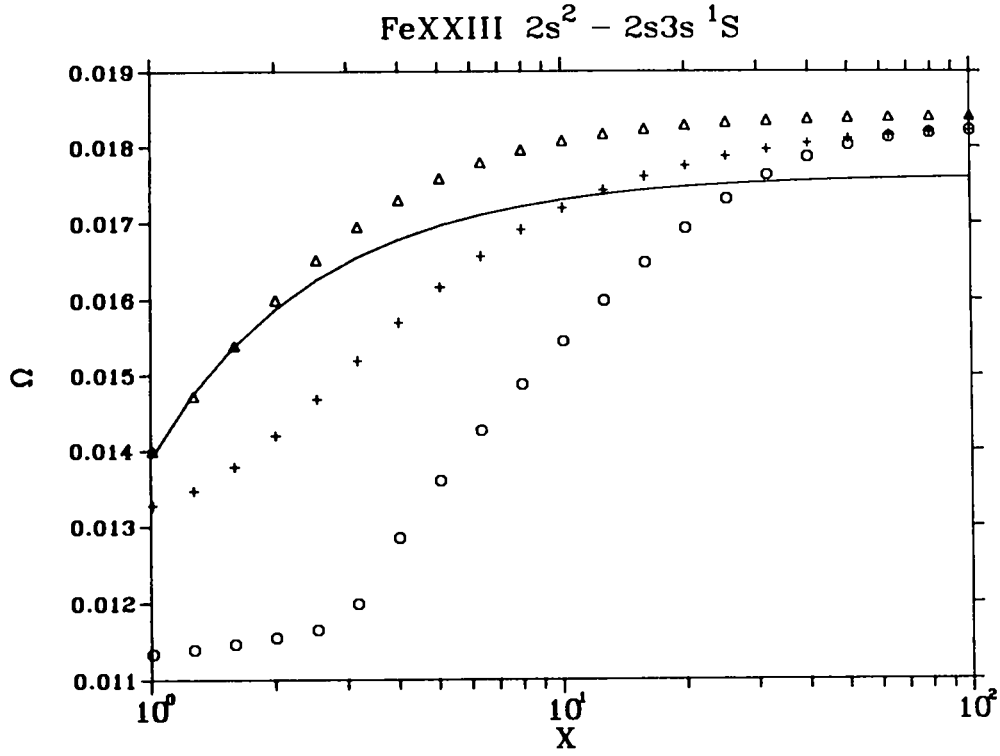

Fig. 13a.

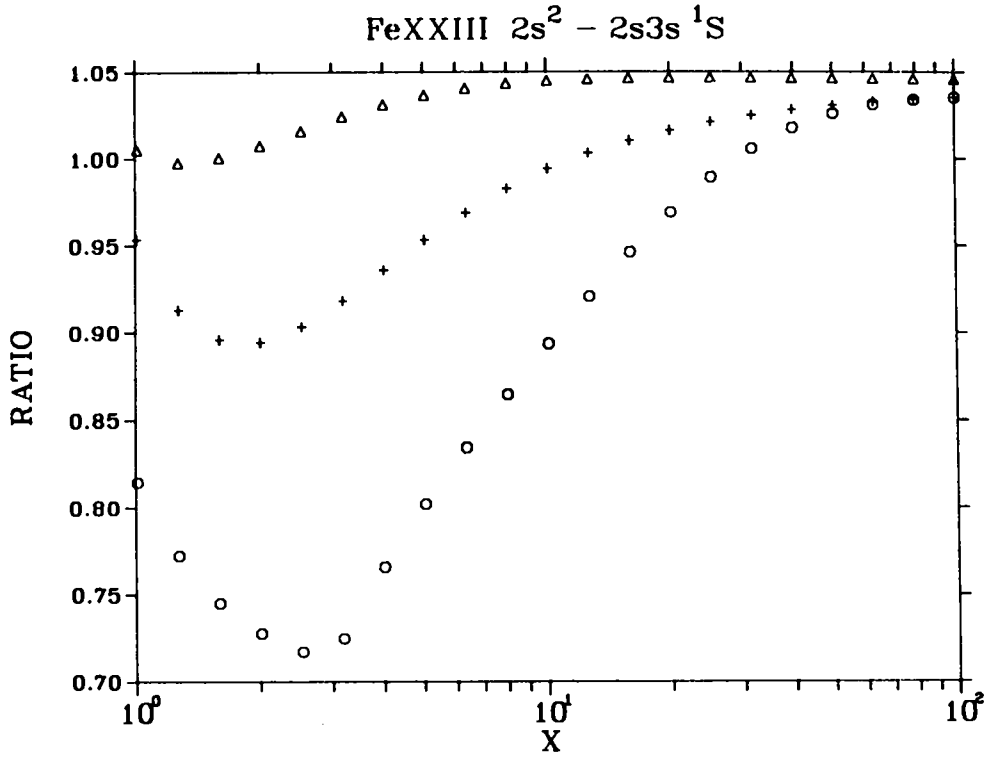

Fig. 13b.

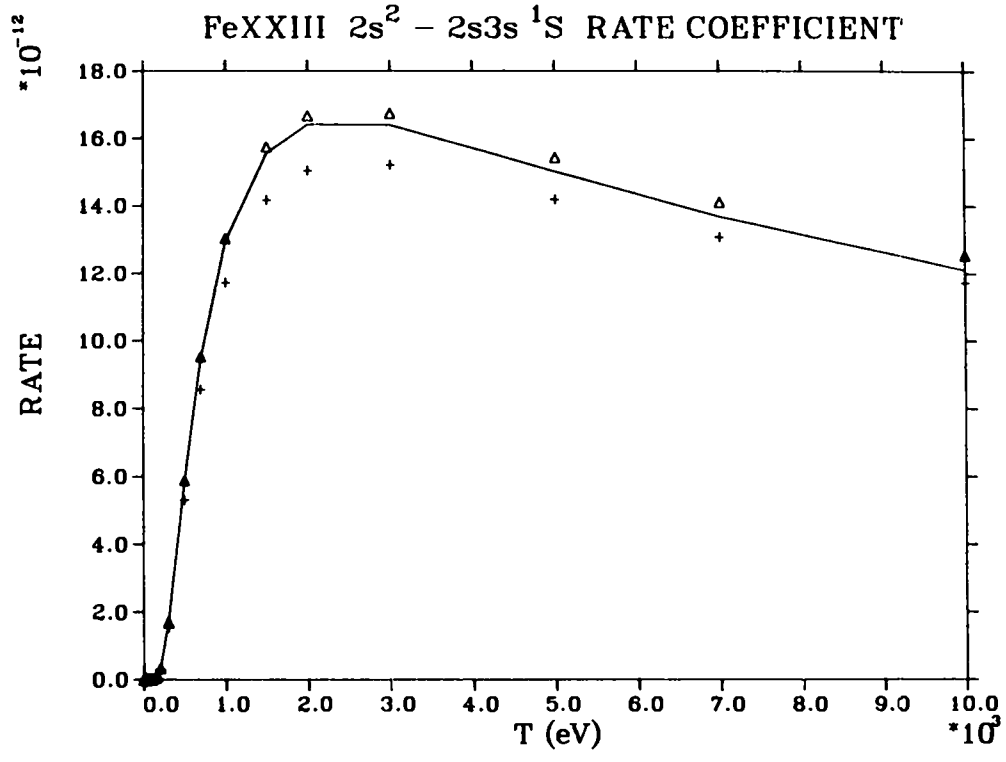

Fig. 13c.

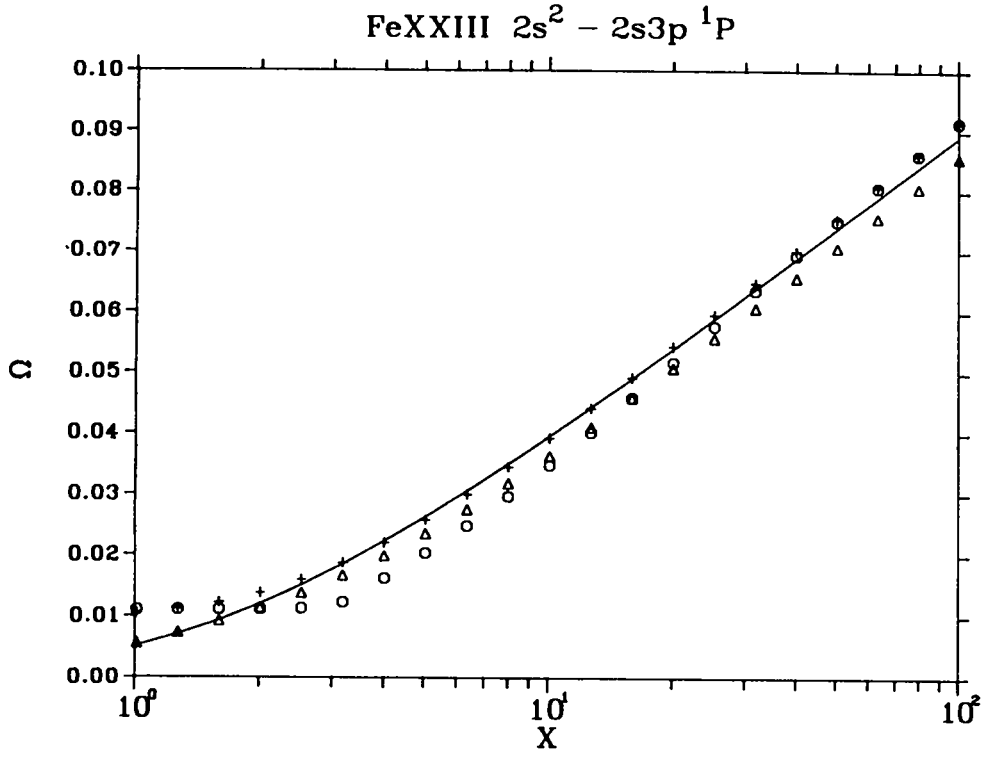

Fig. 14a.

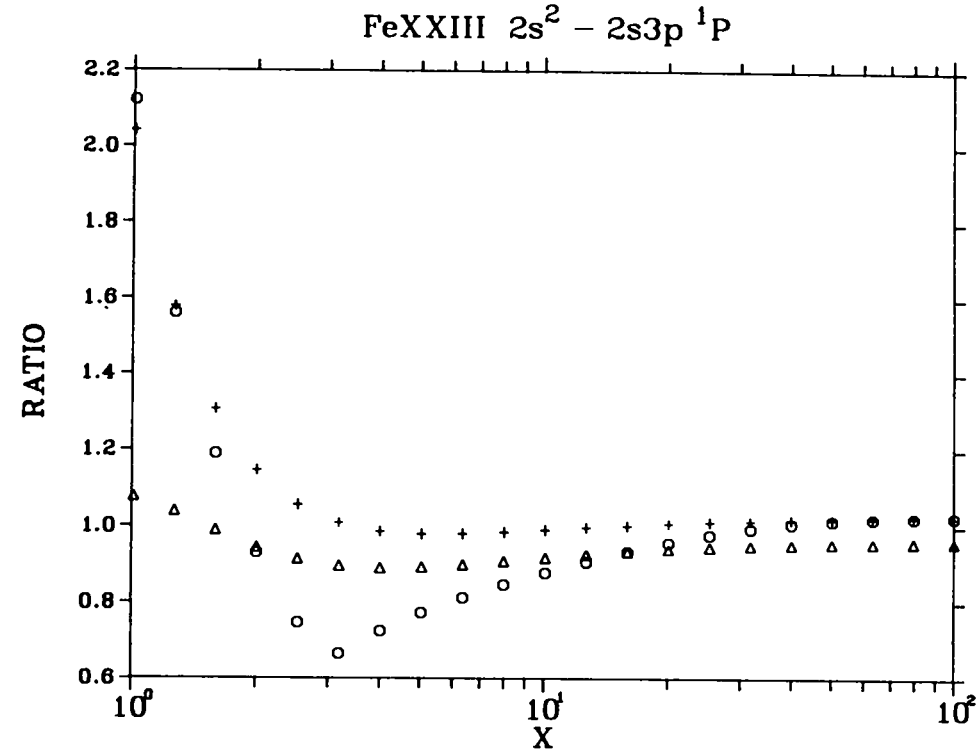

Fig. 14b.

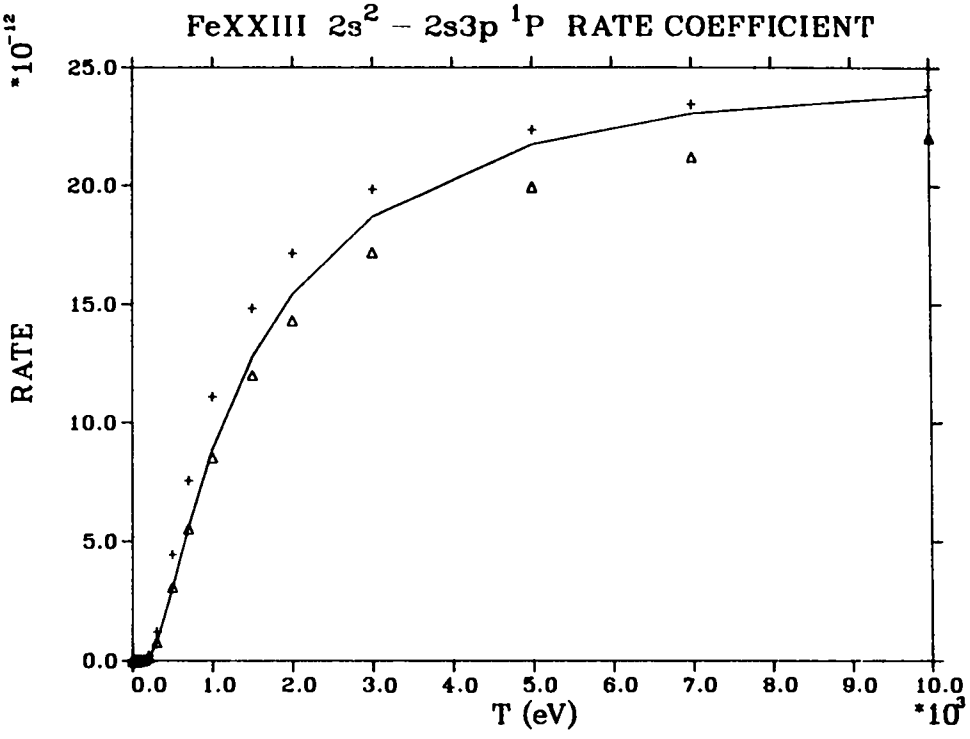

Fig. 14c.

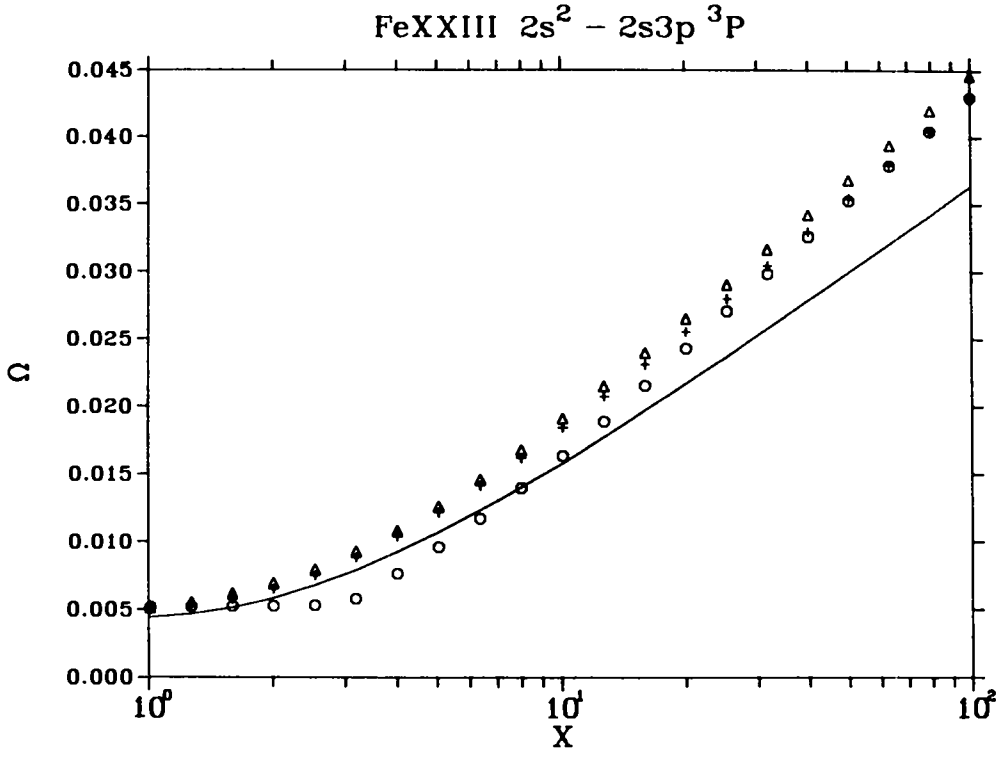

Fig. 15a.

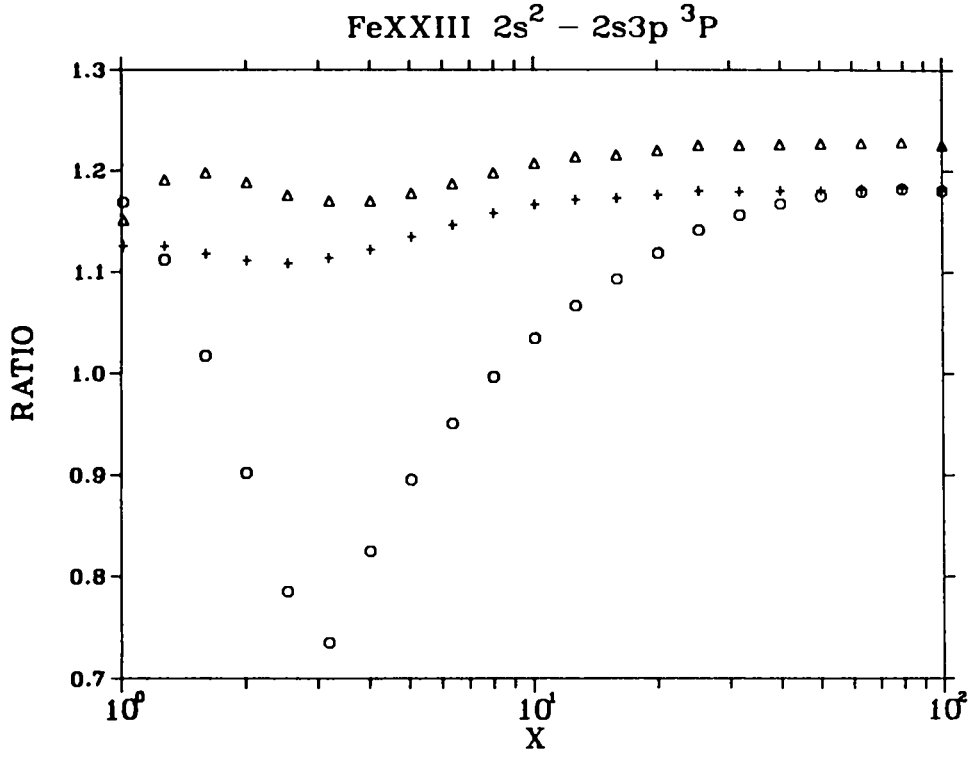

Fig. 15b.

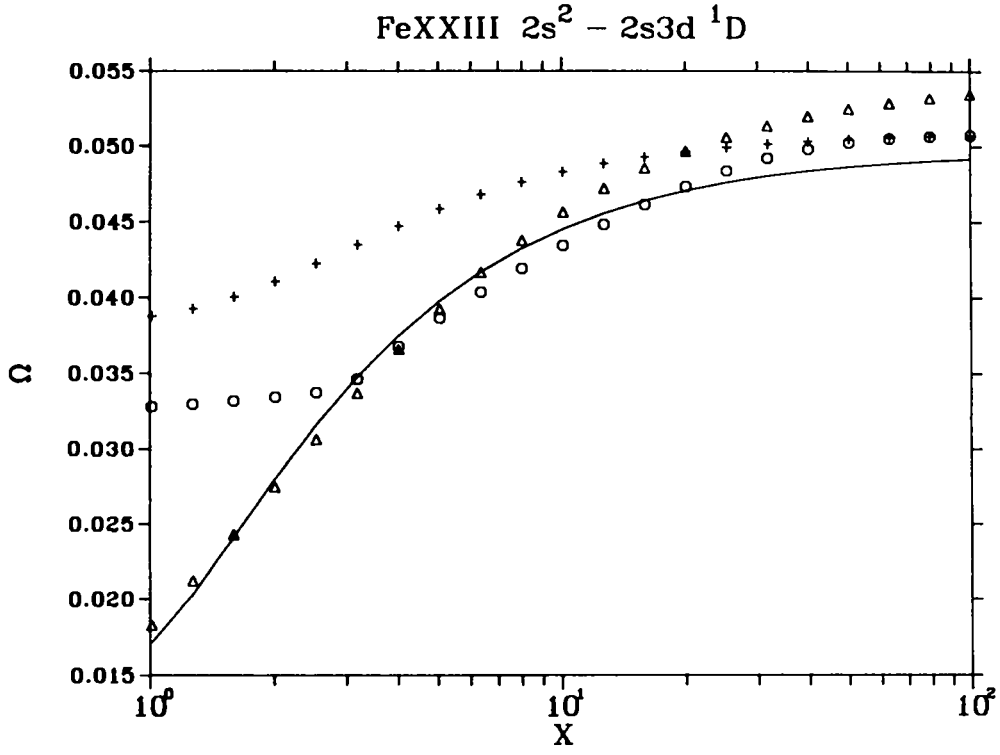

Fig. 16a.

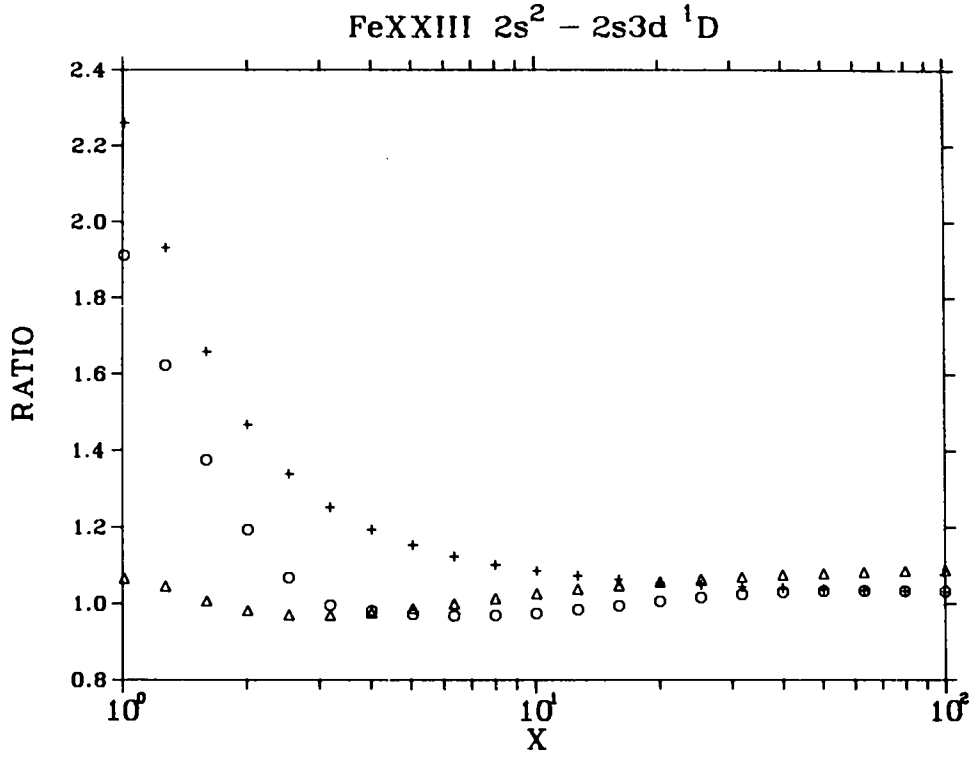

Fig. 16b.

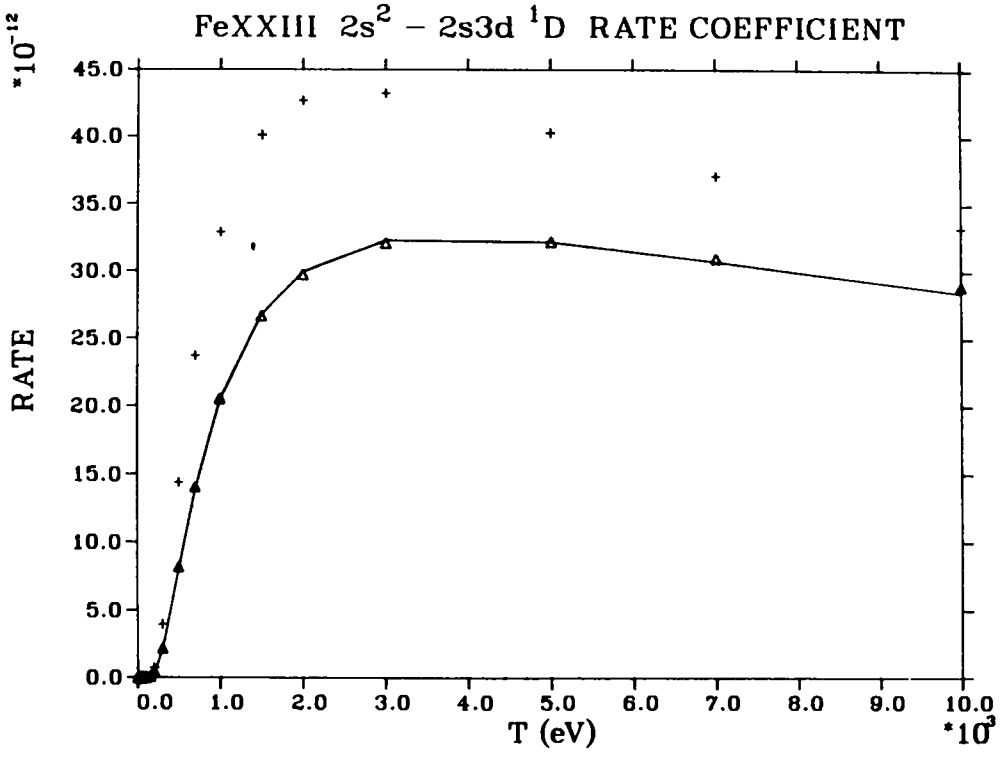

Fig. 16c.

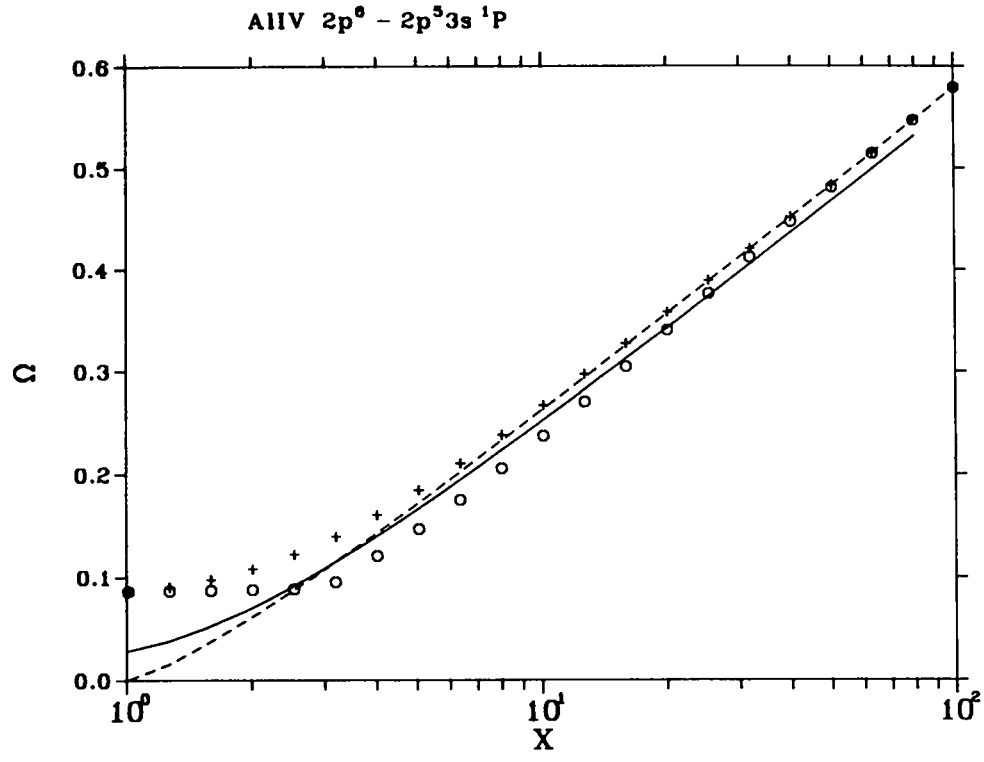
AlIV 2p⁶ - 2p⁵3s ¹P
0.6
0.5
0.4
0.3
0.2
0.1
0.0
Ω
10⁰
10¹
10²
X

Fig. 17.

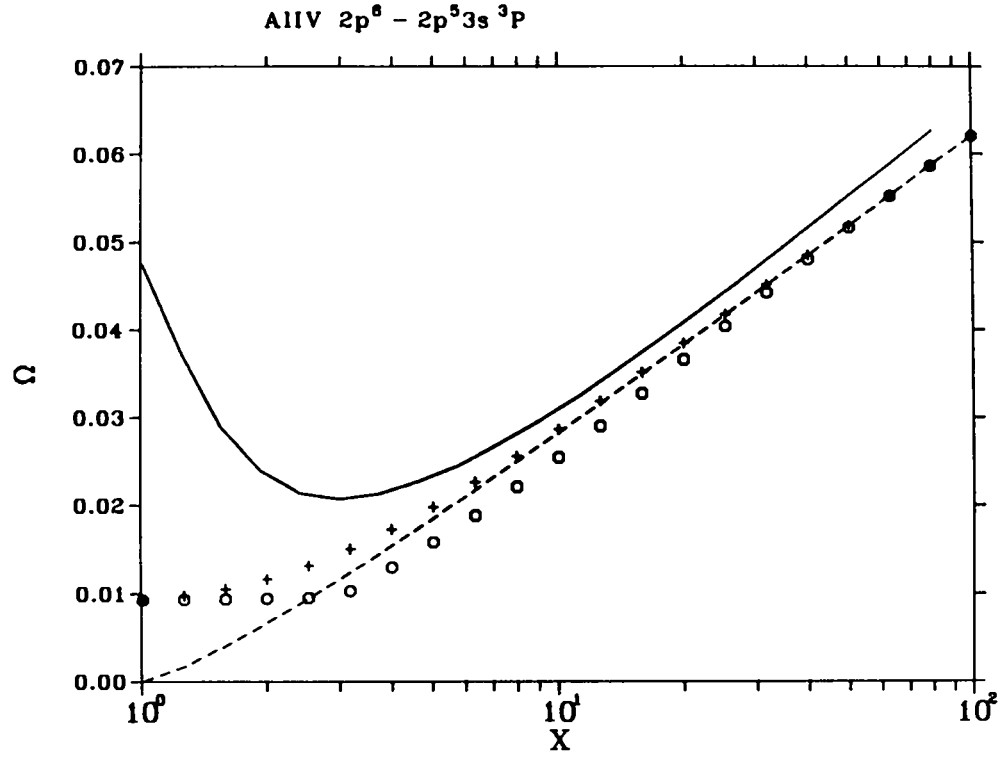
AlIV 2p⁶ - 2p⁵3s ³P
0.07
0.06
0.05
0.04
0.03
0.02
0.01
0.00
Ω
10⁰
10¹
10²
X

Fig. 18.

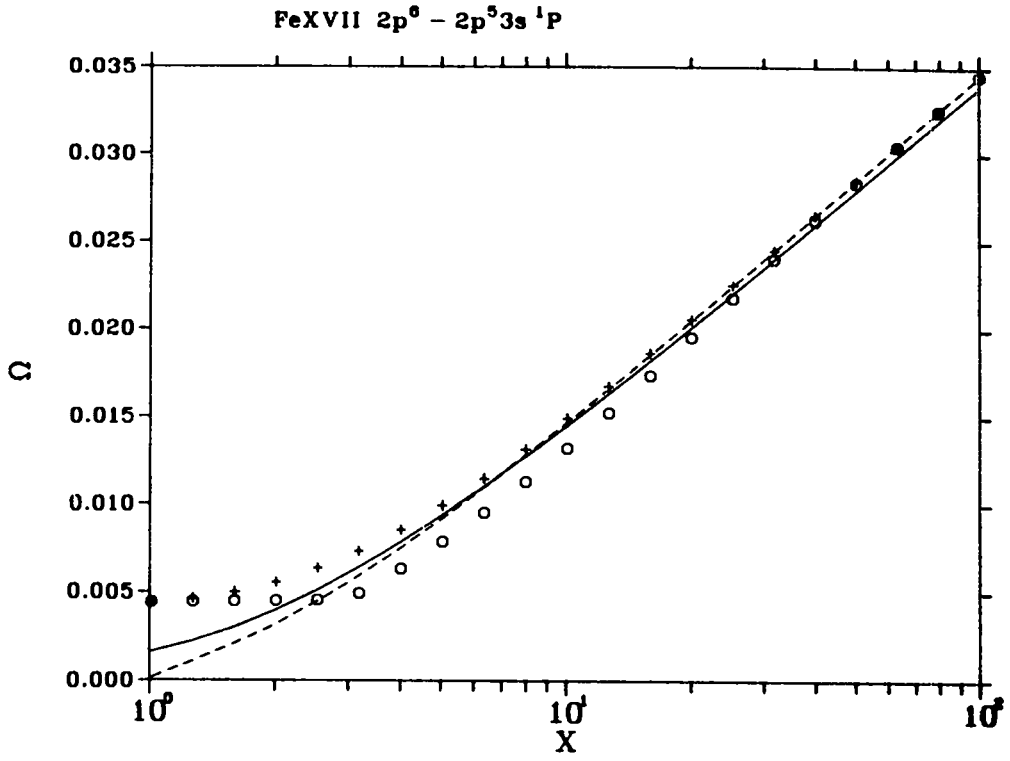

Fig. 19a.

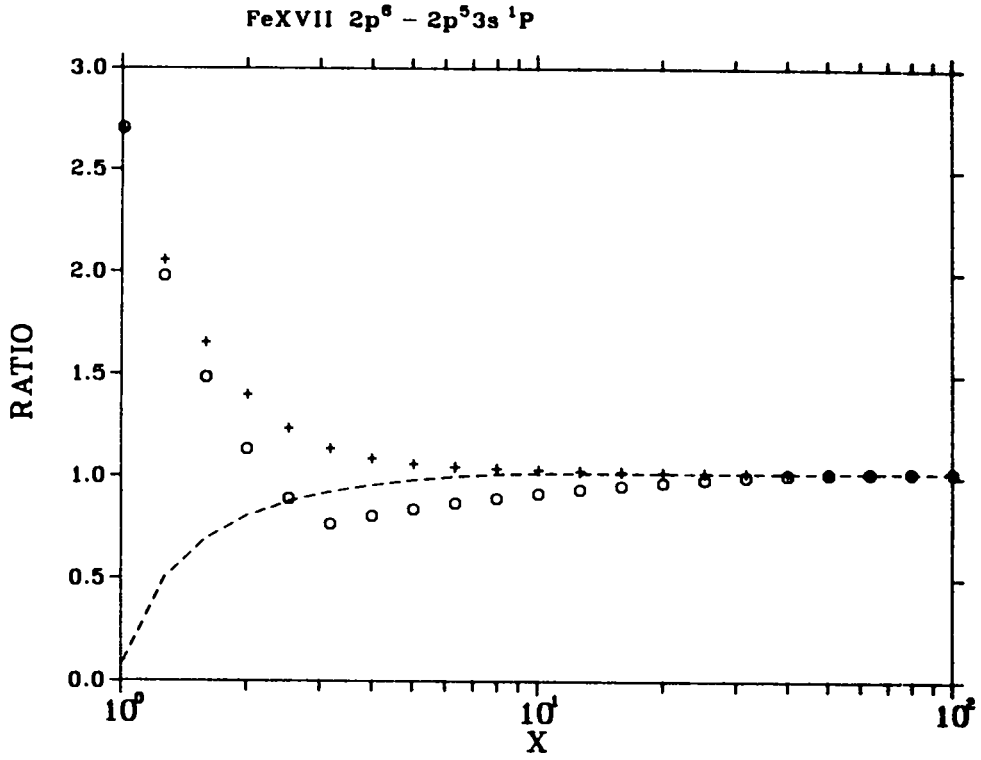

Fig. 19b.

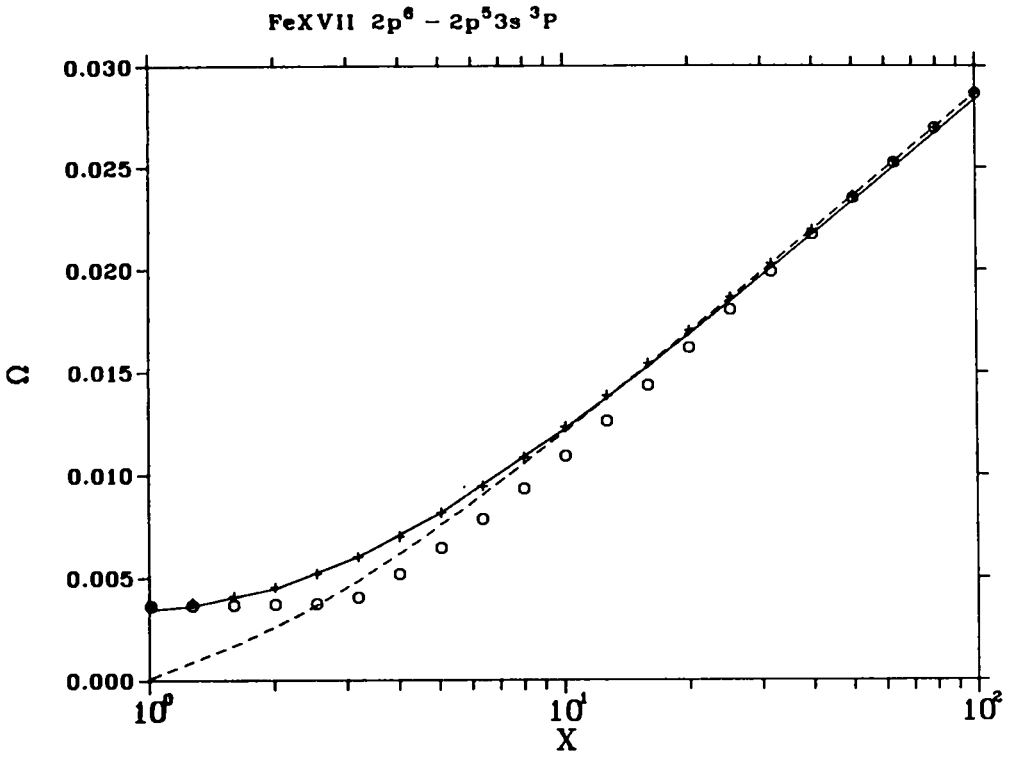

Fig. 20a.

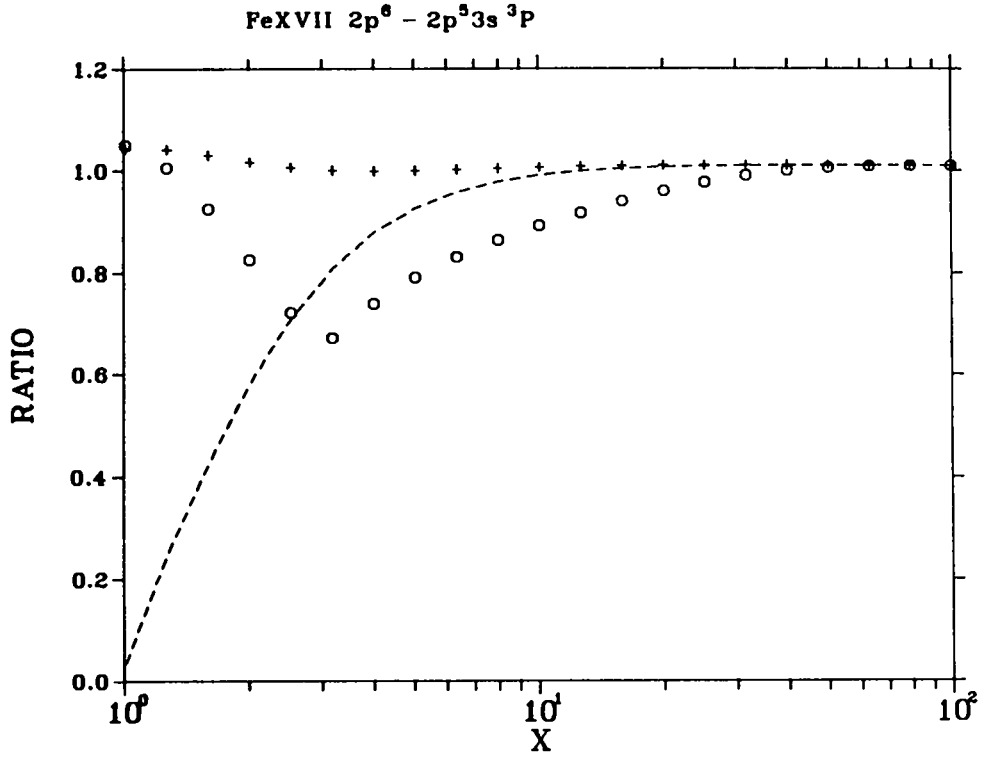

Fig. 20b.

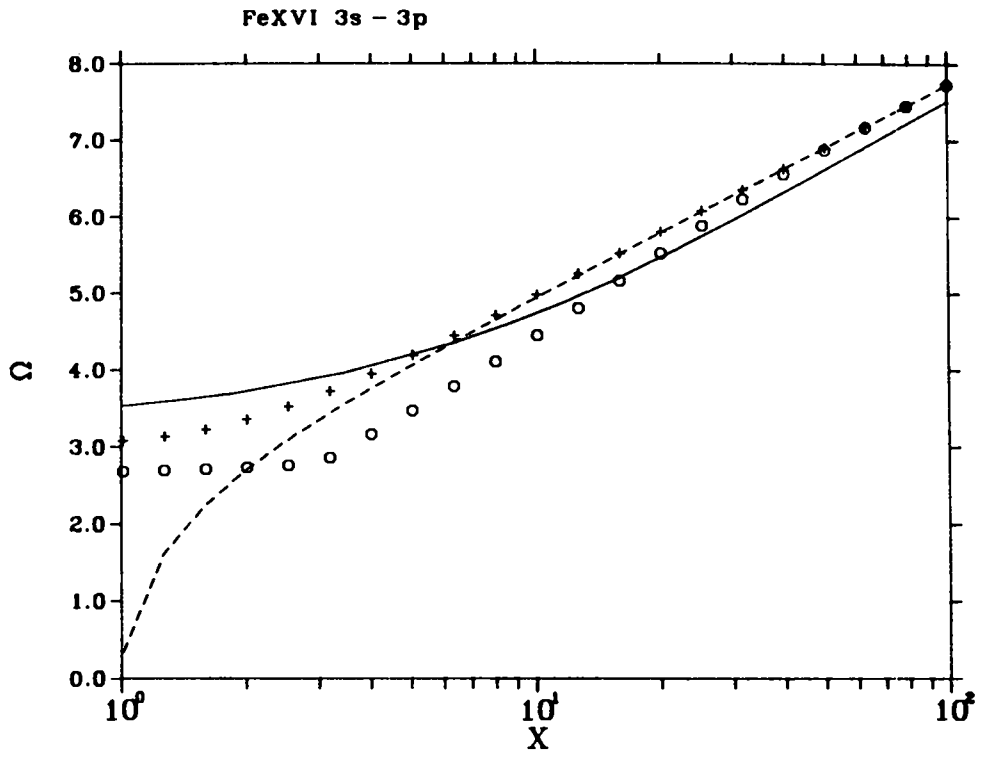
FeXVI 3s – 3p
8.0
7.0
6.0
5.0
4.0
3.0
2.0
1.0
0.0
Ω
10⁰
10¹
10²
X

Fig. 21.

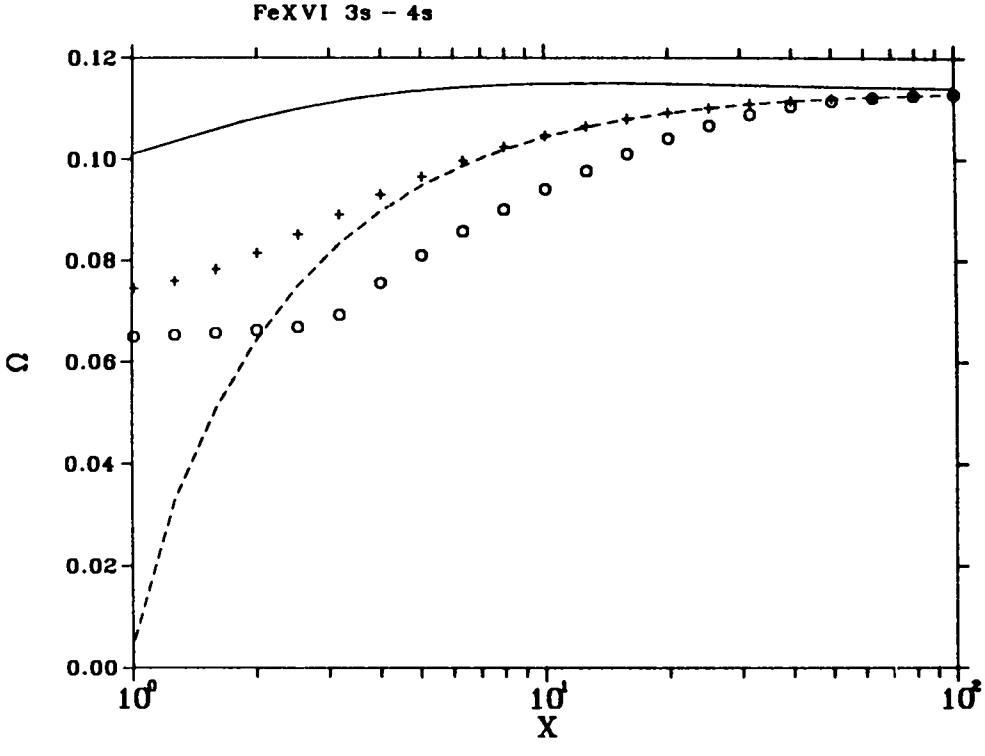
FeXVI 3s – 4s
0.12
0.10
0.08
0.06
0.04
0.02
0.00
Ω
10⁰
10¹
10²
X

Fig. 22.

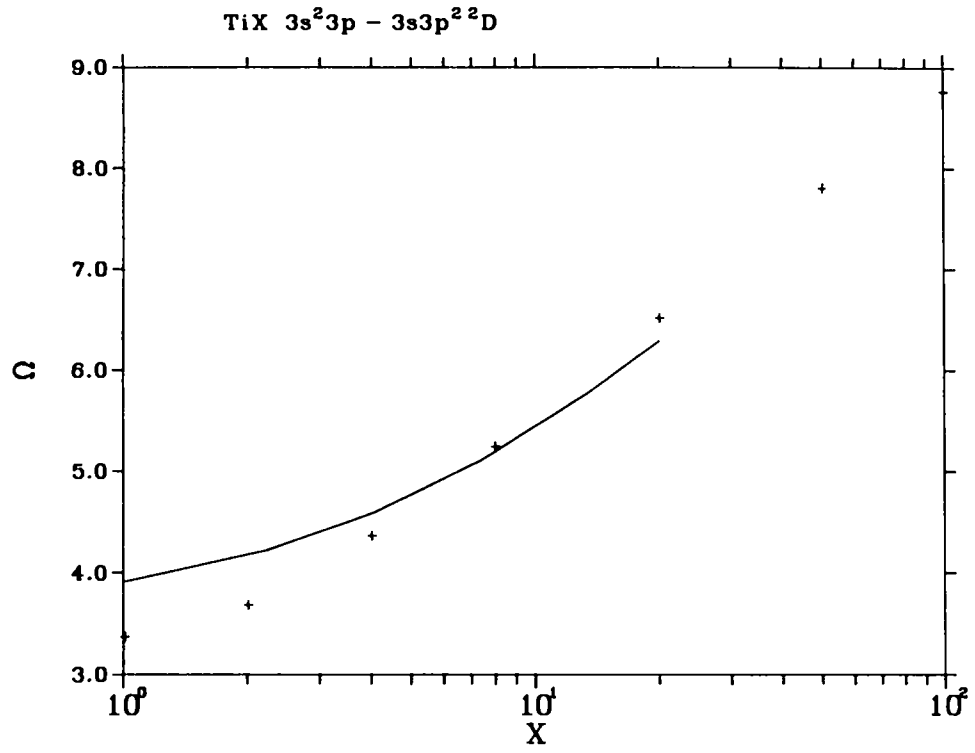
TiX 3s²3p - 3s3p² ²D
9.0
8.0
7.0
6.0
5.0
4.0
3.0
C
10⁰
10¹
10²
X

Fig. 23.

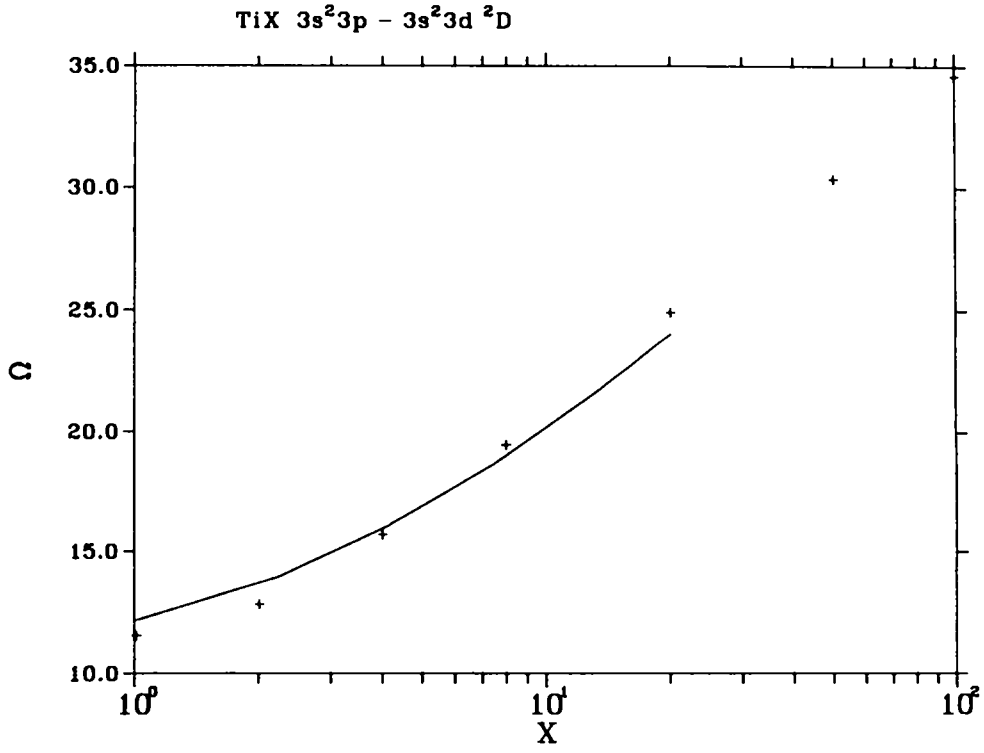
TiX 3s²3p - 3s²3d ²D
35.0
30.0
25.0
20.0
15.0
10.0
C
10⁰
10¹
10²
X

Fig. 24.

Printed in the United States of America
Available from
National Technical Information Service
US Department of Commerce
5285 Port Royal Road
Springfield, VA 22161

Microfiche (A01)

Page Range	NTIS Price Code	Page Range	NTIS Price Code	Page Range	NTIS Price Code
001-025	A02	151-175	A08	301-325	A14
026-050	A03	176-200	A09	326-350	A15
051-075	A04	201-225	A10	351-375	A16
076-100	A05	226-250	A11	376-400	A17
101-125	A06	251-275	A12	401-425	A18
126-150	A07	276-300	A13	426-450	A19
					A20
					A21
					A22
					A23
					A24
					A25
				601-up*	A99

*Contact NTIS for a price quote.

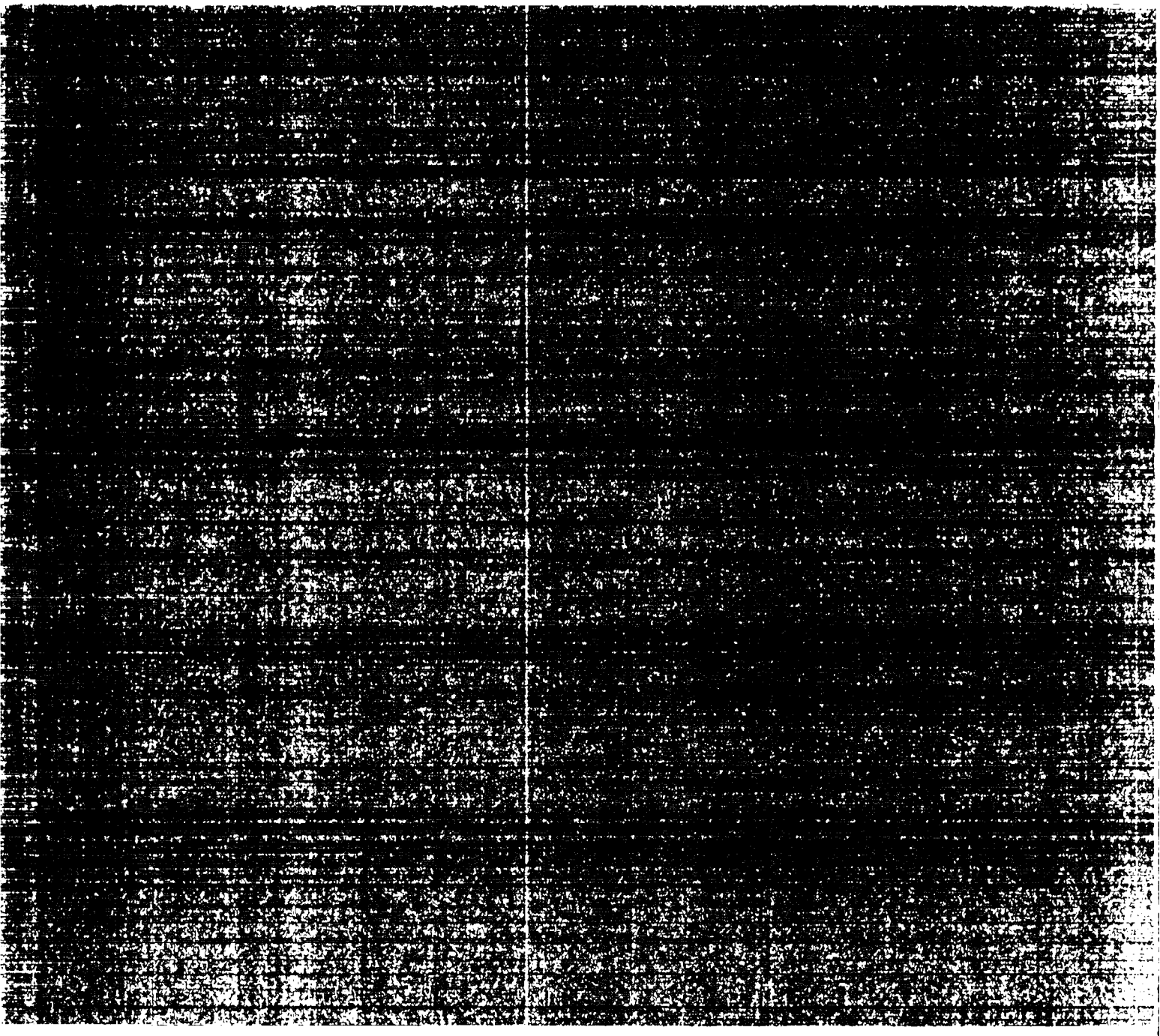

Los Alamos